https://doi.org/10.1093/plcell/koad228 THE PLANT CELL 2023: 35: 4238–4265

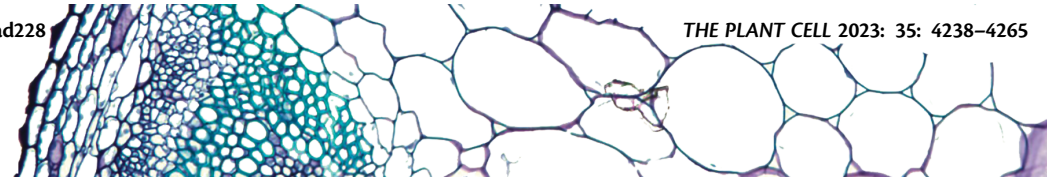

Research Article

MYB24 orchestrates terpene and flavonol metabolism as light responses to anthocyanin depletion in variegated grape berries

Chen Zhang [1,†] Zhanwu Dai [2,†] Thilia Ferrier [3,†] Luis Orduña [1] Antonio Santiago [1] Arnau Peris [1] Darren C.J. Wong [4] Christian Kappel [5] Stefania Savoi [6] Rodrigo Loyola [7] Alessandra Amato [8] Bartosz Kozak [9] Miaomiao Li [10] Akun Liang [11] David Carrasco [12] Carlos Meyer-Regueiro [7] Carmen Espinoza [13] Ghislaine Hilbert [3] Rosa Figueroa-Balderas [14] Dario Cantu [14] Rosa Arroyo-Garcia [12] Patricio Arce-Johnson [15] Patricia Claudel [16] Daniel Errandonea [11] Manuel Rodríguez-Concepción [17] Eric Duchêne [16] Shao-shan Carol Huang [10] Simone Diego Castellarin [9] Giovanni Battista Tornielli [8] Francois Barrieu [3,*,‡] and José Tomás Matus [1,*,‡]

1 Institute for Integrative Systems Biology (I2SysBio), Universitat de València-CSIC, Paterna 46980, Valencia, Spain
2 Beijing Key Laboratory of Grape Science and Enology and Key Laboratory of Plant Resources, Institute of Botany, Chinese Academy of Sciences, Beijing 100093, China
3 EGFV, Bordeaux Sciences Agro, University of Bordeaux, INRAE, ISVV, 210 Chemin de Leysotte, 33140 Villenave d'Ornon, France
4 Ecology and Evolution, Research School of Biology, The Australian National University, Canberra, ACT 2601, Australia
5 Institute for Biochemistry and Biology, University of Potsdam, Potsdam-Golm 14476, Germany
6 Department of Agricultural, Forest and Food Sciences, University of Turin, Turin 10124, Italy
7 Departamento de Genética Molecular y Microbiología, Pontificia Universidad Católica de Chile, Santiago 8331150, Chile
8 Department of Biotechnology, University of Verona, 37134 Verona, Italy
9 Wine Research Centre, University of British Columbia, Vancouver, British Columbia V1V 1V7, Canada
10 Center for Genomics and Systems Biology, Department of Biology, New York University, New York, NY 10003, USA
11 Departamento de Física Aplicada-ICMUV-MALTA Consolider Team, Universitat de València, Burjassot 46100, Valencia, Spain
12 Centre for Plant Biotechnology and Genomics (CBGP), Universidad Politécnica de Madrid-INIA, 28223, Pozuelo de Alarcón, Madrid, Spain
13 Instituto de Ciencias Biomédicas, Facultad de Ciencias de la Salud, Universidad Autónoma de Chile, Santiago 8380453, Chile
14 Department of Viticulture and Enology, University of California Davis, Davis, CA 95616, USA
15 Instituto de Ciencias Aplicadas, Facultad de Ingeniería Universidad Autónoma de Chile
16 SVQV, University of Strasbourg, INRAE, Colmar 68000, France
17 Institute for Plant Molecular and Cell Biology (IBMCP), CSIC-Universitat Politècnica de València, Valencia 46022, Spain

*Author for correspondence: tomas.matus@uv.es (J.T.M.), francois.barrieu@inra.fr (F.B.)
†These authors contributed equally.
‡These authors shared corresponding authorship.
The authors responsible for distribution of materials integral to the findings presented in this article in (https://academic.oup.com/plcell/pages/General-Instructions) are: José Tomás Matus (tomas.matus@uv.es) and Francois Barrieu (francois.barrieu@inrae.fr).

Abstract

Variegation is a rare type of mosaicism not fully studied in plants, especially fruits. We examined red and white sections of grape (*Vitis vinifera* cv. 'Béquignol') variegated berries and found that accumulation of products from branches of the phenylpropanoid and isoprenoid pathways showed an opposite tendency. Light-responsive flavonol and monoterpene levels increased in

Received April 01, 2022. Accepted August 30, 2023. Advance access publication August 30, 2023

anthocyanin-depleted areas in correlation with increasing *MYB24* expression. Cistrome analysis suggested that MYB24 binds to the promoters of 22 terpene synthase (*TPS*) genes, as well as 32 photosynthesis/light-related genes, including carotenoid pathway members, the flavonol regulator *HY5 HOMOLOGUE* (*HYH*), and other radiation response genes. Indeed, *TPS35*, *TPS09*, the carotenoid isomerase gene *CRTISO2*, and *HYH* were activated in the presence of MYB24 and MYC2. We suggest that MYB24 modulates ultraviolet and high-intensity visible light stress responses that include terpene and flavonol synthesis and potentially affects carotenoids. The MYB24 regulatory network is developmentally triggered after the onset of berry ripening, while the absence of anthocyanin sunscreens accelerates its activation, likely in a dose-dependent manner due to increased radiation exposure. Anthocyanins and flavonols in variegated berry skins act as effective sunscreens but for different wavelength ranges. The expression patterns of stress marker genes in red and white sections of 'Béquignol' berries strongly suggest that MYB24 promotes light stress amelioration but only partly succeeds during late ripening.

IN A NUTSHELL

Background: Since plants made the move to land, they have had to adapt to exposure to high-intensity light and ultraviolet radiation. Anthocyanins that accumulate in epidermal cells shield plant tissues from radiation; the absence of these red/purple pigments negatively affects photosynthesis and other physiological processes. We identified and compared pigmented and unpigmented sections of rare, variegated grapevine (*Vitis vinifera*) berries to see whether different light responses were occurring in red and white skin sections.

Question: What are the causes and effects of berry color variegation? Does a central genetic switch contribute to the abundance of phenylpropanoids and isoprenoids in variegated berries? Can we integrate computational analyses and experimental evidence to disentangle these questions?

Findings: White variegation in red-skinned grapevine fruits is caused by the presence of nonfunctional alleles of MYBA1/A2 transcription factors that naturally control anthocyanin biosynthesis. The absence of these pigments enhances a ripening-dependent regulatory network mediated by MYB24 that promotes protection against ultraviolet and high light intensity stress. In response, white skin sections accumulate higher levels of antioxidant monoterpenes and UV-shielding flavonols; however, these compounds only partially ameliorate the detrimental effects of excessive radiation. Genes related to carotenoid metabolism, photosynthesis, and other light signaling responses are bound and directly regulated by MYB24. By conducting in silico and in vitro analyses and using field-grown grapevine plants, we demonstrate that MYB24 orchestrates different specialized metabolism pathways in berry skins in response to increased levels of radiation caused by pigment depletion.

Next steps: Future research should be oriented toward identifying the regulators of MYB24 in order to determine the full regulatory network of MYB24-controlling light responses and late fruit ripening processes.

Introduction

Plants have many specialized metabolites that are pigments. Most of them accumulate as a result of activity of the phenylpropanoid/flavonoid (anthocyanin) and isoprenoid (carotenoid) pathways, 2 of the most studied specialized metabolic pathways in plants. Their presence in flowers and fruits has allowed plants to coevolve with insects and seed dispersers, producing the plethora of color hues and tones found in nature. Beyond this purpose, these compounds also filter harmful excessive radiation and provide accessory photosynthetic capacity, among other roles (Winkel-Shirley 2002).

As pigments, anthocyanins and carotenoids can be used as reliable markers in forward genetics approaches for the identification of genes underlying their biosynthesis. Based on this advantage, extensive progress in understanding the control of flavonoid pigment synthesis has come from studying the combinatorial interaction between activating and repressive sets of R3-MYBs and R2R3-MYBs, beta helix–loop–helix (bHLH), and tryptophan–aspartic acid repeat (WDR) regulators (Albert et al. 2014). WRKY transcription factors (TFs) also interact with these components (Verweij et al. 2016). This "MBW-W" complex (Lloyd et al. 2017) is essential for accumulating anthocyanins and acidifying vacuoles, which promote color changes due to the oxidation/reduction of anthocyanin hydroxyl groups.

Besides flavonoid-regulating MYBs, a few isoprenoid MYB regulators have been identified to date, in *Mimulus lewisii* (Sagawa et al. 2016), kiwifruit (*Actinidia deliciosa*) (Ampomah-Dwamena et al. 2019), tomato (*Solanum lycopersicum*) (Wu et al. 2020), *Freesia hybrida*, and *Arabidopsis thaliana* (Yang et al. 2020). The overexpression of mimulus *RCP1* in a reduced carotenoid pigmentation (*rcp1*) mutant background restored the production of these pigments and surprisingly decreased anthocyanin production by downregulating the expression of *PELAN*, which encodes a MYB activator of anthocyanin biosynthesis. This opposite relationship between anthocyanins and isoprenoids has been observed on very few occasions and in some cases with contradictory verdicts (e.g. in tomato) (Long et al. 2006).

In the case of grapevine (*Vitis vinifera*), white grape varieties seem to have higher carotenoid contents compared with dark-skinned cultivars that accumulate anthocyanins in their berry skins (Bunea et al. 2012). Also, terpenes (a group of volatile isoprenoids giving rich aromas) such as linalool accumulate to higher levels in pink-skinned fruits compared with dark red or black cultivars (Cravero et al. 1994). Another study reported that sesquiterpenes have an antagonistic effect on the accumulation of anthocyanins in grape (Zheng et al. 2021). Altogether, different balances or opposite relationships between anthocyanins and certain isoprenoids seem to exist in the grape berry. Whether this relationship depends on transcriptional regulation remains uncertain.

Grapes constitute a rich source of specialized metabolites and thus represent an interesting model to compare the abundance of metabolites from different pathways, particularly as they are all quantitatively influenced by the environment. In the case of pigmented cultivars, anthocyanins begin to accumulate at the onset of ripening (i.e. the widely used French term *véraison*) in epidermal and subepidermal cell layers that constitute the berry skin (corresponding to L1 and L2 cell types) or also in the flesh (L2) in the case of '*teinturier*' cultivars. Their accumulation increases in response to light and ultraviolet radiation (Matus et al. 2009, 2017) but declines at high temperatures (Mori et al. 2007). Mono- and sesquiterpene levels vary greatly amongst grape cultivars, although a vast majority accumulates at the end of the ripening stage and is highly influenced by temperature (Wen et al. 2015), light (Zhang et al. 2017), UV-B (Carbonell-Bejerano et al. 2014), and water deficit (Savoi et al. 2016). Finally, carotenoid levels decline progressively throughout berry skin development (a sharp decrease occurs at veraison [V]) (Young et al. 2012), but this tendency is arrested and inverted with high radiation levels (Joubert et al. 2016).

The activation of the anthocyanin pathway in the fruit of grapevine depends on the allelic conditions of the *R2R3-MYBA1* and *MYBA2* regulators located at the berry color locus (Kobayashi et al. 2004). One of the most frequent white skin phenotypes results from the insertion of the *Gret1* retrotransposon in the 5′ untranslated region (UTR) of *MYBA1* (Kobayashi et al. 2004) and the concomitant nonsynonymous single-nucleotide mutations in the *MYBA2* coding region (Walker et al. 2007). Due to its transposable nature, the insertion/excision of *Gret1* can often occur, leading to somatic mutations in a single cell. If these occur and proliferate in meristematic tissue, pigment mutants can arise as bud sports. Vegetative propagation is widely used for grapes; therefore, bud sports and their novel traits can be selected and retained by breeders. In addition, if somatic mutations occur in restricted cell lineages, variegated phenotypes can be observed (Foster and Aranzana 2018). Berry color depletion and reversion are often observed in vineyards; however, mosaicism or chimerism (i.e. forms of variegation) is somewhat rare in grapevine, and their molecular study remains limited.

Here, we describe the occurrence of natural berry color variegation in the black-skinned grape cultivar 'Béquignol Noir (B. Noir)'. We compared red and white berry skin sections to understand the origin and consequences of this color alteration. The use of a likely isogenic background (the only difference being the allelic composition at the berry color locus) provides compelling evidence of the inverse accumulation of specific phenylpropanoids and isoprenoids in response to MYBA1/MYBA2 inactivation and establishes a transcriptional association between these 2 different specialized metabolic pathways in plants. We show that variegation transcriptionally promotes the accumulation of a battery of different specialized metabolites that could filter radiation and/or control oxidative damage. Our results point to MYB24 as an important modulator of this response.

Results

Variegated berries lose the capacity to accumulate anthocyanins in white skin sections due to inactivation of MYBA1 and MYBA2

The grape cultivar (cv.) 'Béquignol' is found in Bordeaux and southwest regions of France and has a high predisposition for producing bud sports. This varietal group is composed of 3 recognized somatic variants: the red/black-skinned cv. 'B. Noir', the pale-colored cv. 'Béquignol Gris (B. Gris)', and the unpigmented 'Béquignol Blanc (B. Blanc)' (Supplemental Fig. S1A). In addition to these variants, cv. 'B. Noir' vines present an infrequent pigment alteration in some of their berries, occurring in around 53% of the clusters and in about 4% of the berries within those clusters. These berries exhibit uneven skin pigmentation throughout all ripening stages, with small-to-large white or red stripes. In some other cases, half-colored berries are also found (Fig. 1A and Supplemental Fig. S1B).

We compared transverse sections of variegated berries, sampled at 5 wks after V (5WAV) by optical microscopy (Fig. 1, B to D). As seen in both cv. 'B. Noir' unvariegated and pigmented variegated berries, skins consist of several layers of anthocyanin-accumulating cells. Large and vacuolated subepidermal cells accumulating both reddish and purplish anthocyanin vacuolar inclusion (AVIs) were discernable in pigmented sections. In contrast, anthocyanins were absent in L1 and L2 cell layers of the white skin sections of unvariegated berries. In the variegated berries, the boundaries between pigmented and unpigmented areas were clearly distinguishable. As surveyed by HPLC quantification, anthocyanin derivatives were only present in pigmented berry skins. These were similar in terms of total abundance and the relative proportion of di-/trihydroxylated forms in both unvariegated berries of cv. 'B. Noir' and the red skin sections of variegated berries (minor abundance changes were affected by vintage even though the proportions of each derivative were not affected; Supplemental Fig. S2).

The color of the grape berry skin relies on the allelic condition of a major locus on chromosome 2 that harbors the genes encoding the anthocyanin-promoting TFs R2R3-MYBA1 and MYBA2. Thus, we investigated whether these TFs could

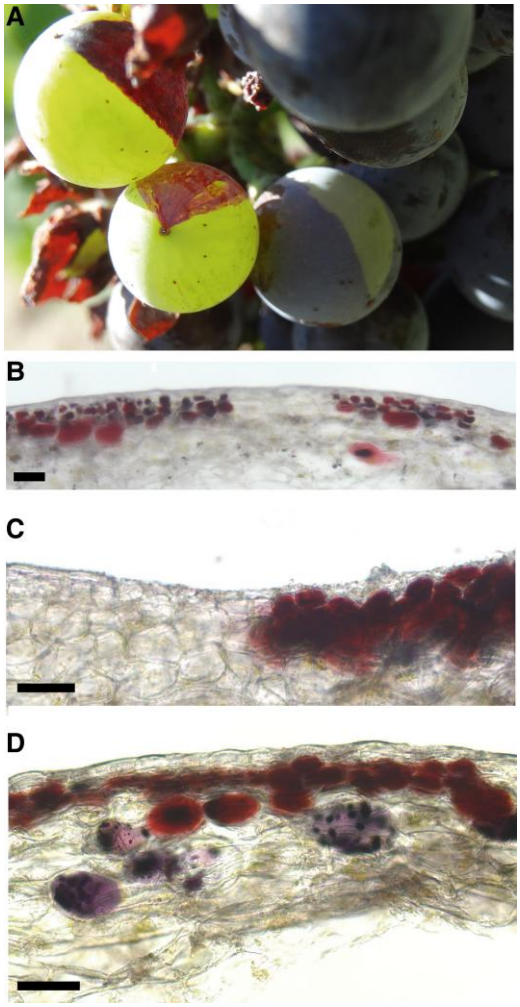

Figure 1. Differential skin pigmentation as a result of anthocyanin depletion in variegated cv. 'B. Noir' berries. **A)** Irregular berry skin pigmentation observed in field-grown vines at 2WAV. **B)** to **D)** Light microscopy images of variegated berry skin cell layers. **C)** and **D)** Subepidermal cells near color transitions show AVIs accumulating either reddish or purplish pigments corresponding to di- and trihydroxylated anthocyanin derivatives, respectively (see also Supplemental Fig. S2A). Pigment accumulation in variegated berries is seen throughout fruit ripening. Pigment accumulation in nonvariegated cv. 'B. Noir', 'B. Gris', and 'B. Blanc' fruits can be seen in Supplemental Fig. S1. Bar scale: 5 μm.

explain this variegation phenotype. The inactivation of *MYBA1* through the insertion of the *Gret1* retrotransposon in the promoter/5′ UTR (Kobayashi et al. 2004) and nonsynonymous single-nucleotide polymorphisms (SNPs) in the *MYBA2* coding region (Walker et al. 2007) account for the unpigmented phenotype of most white-skinned cultivars known to date. Reversions from nonfunctional to functional alleles largely occur by excision of *Gret1* in the form of somatic mutations that occur independently in L1 or L2 layers of floral meristems within buds. Since different plant organs and tissues are derived from the L1 and L2 meristem layers, we conducted a cell layer–specific molecular characterization of the berry color locus. Eleven molecular markers in genomic DNA (gDNA) extracted from L1 + L2 (berry skins and leaves) and L2 (berry pulp and roots)-derived organs were assessed from all somatic variants of the 'Béquignol' family (Fig. 2A). This haplotype structure analysis revealed a recessive homozygous (hm) L2 layer configuration in 'B. Blanc' and 'B. Gris', both bud sports of 'B. Noir' that in turn present a heterozygous (hz) functional allele in this cell layer. This suggests that mutations in L2 are rather common in bud sports and, based on other studies, are probably more widespread than somatic mutations in L1 (Ferreira, Pinto-Carnide, et al. 2018). The white skin layer of the variegated berry shows an hm haplotype for the white allele, corroborated with the null expression of *MYBA1* and its target *UFGT1* (Fig. 2B). Despite this genetic makeup being identical to that of 'B. Blanc', the variegated red skin area matches the genetic profile of nonvariegated 'B. Noir' berries.

Considering the 2 genetic scenarios of L1 cells in 'B. Noir', we developed 2 models for the rise in variegation that can even occur concomitantly. The first considers a somatic recombination event occurring in the L2 cell layer generating the hm white haplotype. This is subsequently incorporated into the L1 layer by displacement, providing a "patch" presence of nonfunctional loci. The second model proposes that somatic mutations occur independently in both layers, where cells with nonfunctional alleles would gradually overlap between layers, leading to white skin sections. The L2 to L1 displacement resembles the sequential model proposed for explaining the formation of cv. 'Shalistin' (Walker et al. 2006), while independent mutations occurring in L1 and L2 leading to nonfunctional alleles have been suggested in the formation of cv. 'Pinot Blanc' and 'Pinot Gris' (Vezzulli et al. 2012). In all these cases, however, the mutated cells occupy the entire layer, leading to periclinal chimeras.

Lack of anthocyanins and loss of MYBA1/A2 activity correlate with expression changes in phenylpropanoid and isoprenoid pathway genes and additional R2R3-MYB TFs

We compared the transcriptomes of variegated red and white skin sections of cv. 'B. Noir' using Operon oligonucleotide microarrays (with ∼15,000 genes represented; Supplemental Data Set S1). The analysis was conducted on grape skins at the midripening stage of 5WAV (Supplemental Data Set 2) and showed 807 genes that are significantly differentially expressed (DE) in response to anthocyanin depletion (Supplemental Data Set 3), including 454 red skin upregulated genes (RUGs, all with fold change (FC) $\geq$ 1.3) and 353 white skin upregulated genes (WUGs, all with FC $\geq$ 1.3). Gene set enrichment analysis (GSEA; Supplemental Data Set 4) and category enrichment analysis (MapMan Wilcoxon test $P < 0.01$; Supplemental Data Set 5) showed that RUGs were enriched in phenylpropanoid pathway terms, including lignin and flavonoid (anthocyanin) biosynthesis and response to heat processes. Meanwhile, many photosynthesis-related terms (e.g. light reaction, photosystem I and II, and chlorophyll metabolic

A

Molecular marker and genomic coordinate on chromosome 2 (in Mb)

			SC8_010		SC8_026		VVNTM1		VvMybA2		VvMybA1		VVNTM3		VVNTM5		VVNTM6		VVNTM4		VVIU20		VMC7G3	
Cultivar	Organ	Cell layer	12674		12970		14149		14181		14248		14288		14325		14330		14384		16539		18270	
B. Noir	Root	L2	121	123	250	256	165	171	T	G	Gret	Non-Gret	274	298	283	289	149	151	208	210	365	368	116	116
B. Noir	Leaf	L1+L2	121	123	250	256	165	171	T	G	Gret	Non-Gret	274	298	283	289	149	151	208	210	365	368	116	116
B. Noir-variegated	Red skin section	L1+L2	121	123	250	256	165	171	T	G	Gret	Non-Gret	274	298	283	289	149	151	208	210	365	368	116	116
B. Noir-variegated	White skin	L1+L2	121	121	256	256	171	171	T	T	Gret	Gret	274	274	289	289	151	151	208	210	365	368	116	116
B. gris	Root	L2	121	121	256	256	171	171	T	T	Gret	Gret	274	274	289	289	151	151	208	210	365	368	116	116
B. gris	Leaf	L1+L2	121	123	250	256	165	171	T	G	Gret	Non-Gret	274	274	283	289	151	151	208	210	365	368	116	116
B. gris	Pulp	L2	121	121	256	256	171	171	T	T	Gret	Gret	274	274	289	289	151	151	208	210	365	368	116	116
B. gris	Skin	L1+L2	121	123	250	256	165	171	T	G	Gret	Non-Gret	274	274	283	289	151	151	208	210	365	368	116	116
B. blanc	Root	L2	121	121	256	256	171	171	T	T	Gret	Gret	274	274	289	289	151	151	208	210	365	368	116	116
B. blanc	Leaf	L1+L2	121	121	256	256	171	171	T	T	Gret	Gret	274	274	289	289	151	151	208	210	365	368	116	116
B. blanc	Pulp	L2	121	121	256	256	171	171	T	T	Gret	Gret	274	274	289	289	151	151	208	210	365	368	116	116
B. blanc	Skin	L1+L2	121	121	256	256	171	171	T	T	Gret	Gret	274	274	289	289	151	151	208	210	365	368	116	116

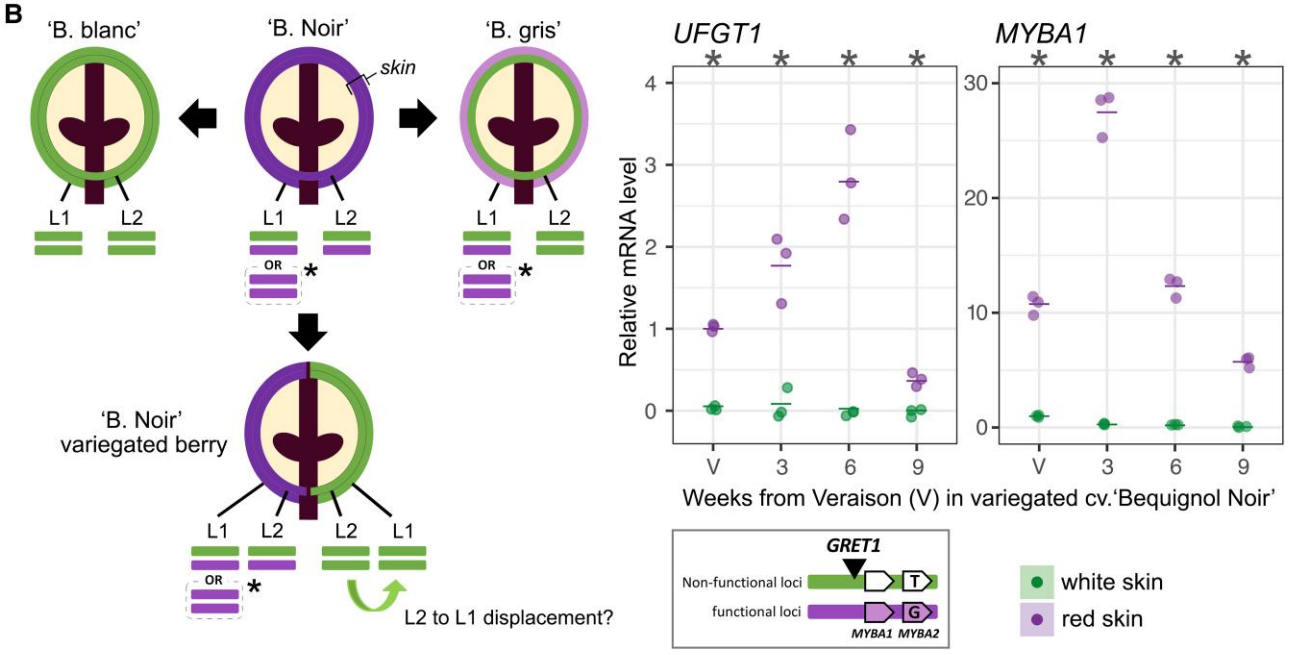

Figure 2. Haplotype structure analysis of the berry color locus reveals 2 different genotypes in a single variegated berry of cv. 'B. Noir'. **A)** Genetic profiling of the berry color locus and its surrounding genomic region in color somatic variants, including white, grey, red, and variegated berries of 'Béquignol' cultivars. Eight microsatellite markers were assessed across the distal arm of chromosome 2, including allele sequence analysis of the anthocyanin regulators *MYBA1* and *MYBA2* (allele sizes are shown in base pairs). *MYBA1– Gret1* and *MYBA2–T* are the nonfunctional alleles, while *MYBA1–non-Gret1* and *MYBA2–G* correspond to the functional alleles. Allele size is shown in bp. **B)** Left panel: model for the formation of 'B. Blanc', 'B. Gris', and the variegated phenotype from independent somatic mutation events in 'B. Noir'. Structural dynamics at the berry color locus in L1 and L2 meristematic cell layers are indicated for each variant. Asterisks represent an alternative configuration for both alleles in the L1 layer. **B)** Right panel: expression profiles of *UFGT1* and its target *MYBA1* at different ripening stages in red and white skin sections of variegated berries. Sixteen berries from 8 clusters from 5 plants were used per biological replicate. Data from 3 biological replicates are shown (averages as horizontal lines). Asterisks indicate significant differences ($P < 0.05$) between skin sections based on 1-way ANOVA followed by Tukey's post hoc test performed independently for each stage.

processes) and the carotenoid pathway were significantly enriched within WUGs (Fig. 3, A and B; Supplemental Fig. S3). WUGs were also associated with other isoprenoids (e.g. terpenes and gibberellins) and response to abiotic stimulus (e.g. light and radiation) (Fig. 3A). In the RUG and WUG lists, several DE TF genes were present, mostly belonging to the R2R3-MYB family. *MYBA1* and the shikimate/stilbene pathway regulator *MYB15* (Orduña et al. 2022) were induced in red skin areas, while the flavonol regulator *MYBF1* (Czemmel et al. 2009), the stomata opening regulator *MYB60* (Galbiati et al. 2011), and a still-uncharacterized *MYB24* homologue were induced in anthocyanin-devoid sections (Fig. 3C).

Taking advantage of the large amount of public transcriptomic data available for *Vitis* sp. and the gene coexpression analyses generated with this data (Orduña et al. 2022, Orduña et al. 2023) and presented in our Vitis Visualization (VitViz) platform (http://www.vitviz.tomsbiolab.com/) (Navarro-Payá et al. 2022), we explored the

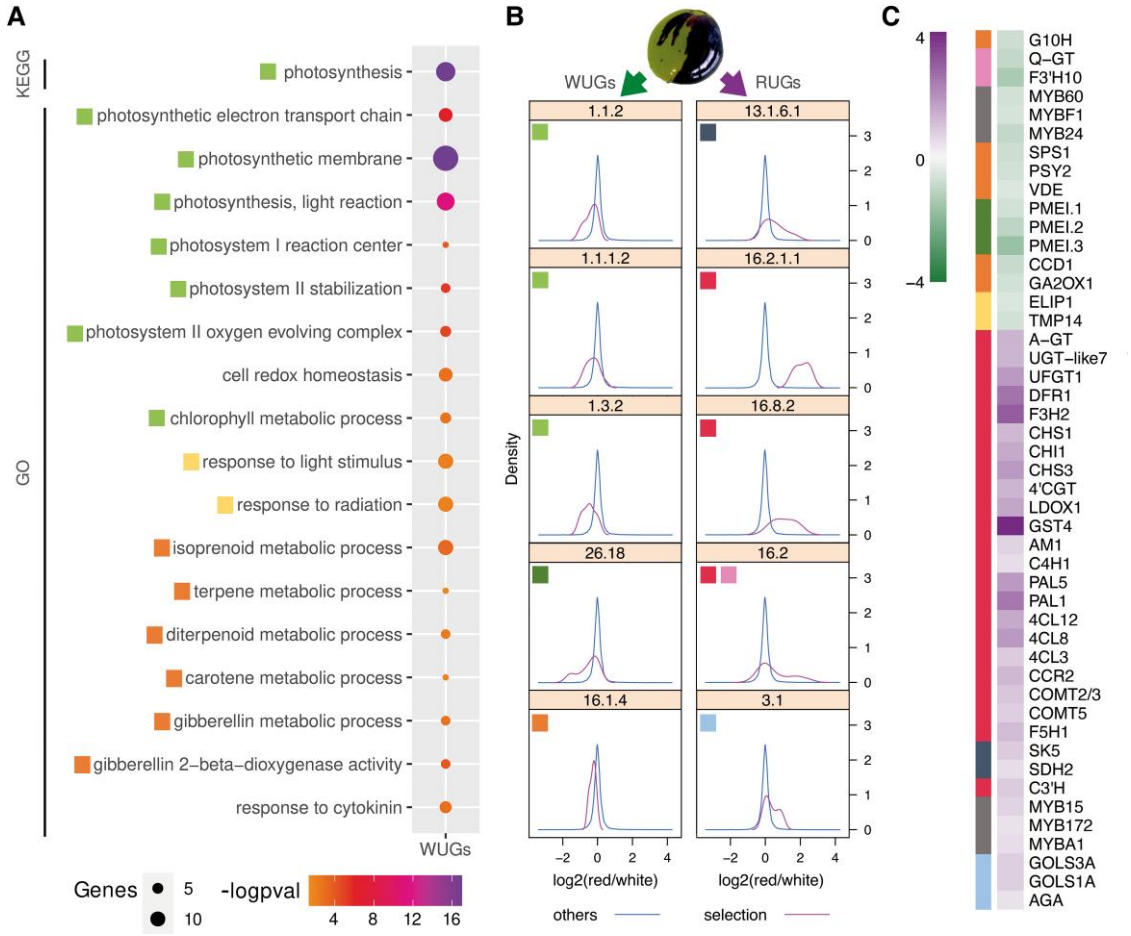

Figure 3. Transcriptomic landscapes of inversely pigmented sections of variegated berries show different pathways perturbed by MYBA1/MYBA2 inactivation. **A)** A selection of significantly enriched terms from Kyoto Encyclopedia of Genes and Genomes (KEGG) and GO ontologies in WUGs. The -logpval scale represents statistical significance on a continuous color scale from orange to purple. The number of WUGs intersecting with each ontology term is indicated by point size. **B)** Density plots of functional MapMan ontologies in berry skin transcriptomes illustrating shifts in differential gene expression. Significantly affected categories (bins) were determined based on Wilcoxon test (false discovery rate [FDR] < 0.05). Bins: 1.1.2 light reaction, photosystem I; 1.1.1.2 light reaction, photosystem II (polypeptide subunits); 1.3.2 Calvin cycle, Rubisco small subunit; 26.18 invertase/pectin methylesterase inhibitor family protein (misc.); 16.1.4 sary metabolism, isoprenoids, carotenoids; 13.1.6.1 aromatic amino acid metabolism, chorismate; 16.2.1.1 lignin biosynthesis, PAL; 16.8.2 flavonoids, chalcones; 16.2 sary metabolism, phenylpropanoids; 3.1 minor CHO metabolism, raffinose family. Other significant categories can be found in **Supplemental Data Set 5**. **C)** Log2 expression ratios of selected genes belonging to significant categories illustrated by colored boxes found in **A)** and **B)**. Gene IDs and expression values are found in **Supplemental Data Set 6**.

potential gene regulatory mechanisms of the few TF genes DE among WUGs (*MYB24*, *MYBF1*, and *MYB60*). We constructed aggregate gene coexpression networks (GCNs) with condition-dependent (flower/fruit; 35 Sequence Read Archive [SRA] studies, 807 data sets/runs) and condition-independent (all organs; 131 SRA studies, 2,767 data sets) data (Supplemental Data Set 7) and analyzed them by GSEA (Supplemental Data Set 8). In the condition-dependent data, MYB60-GCN was enriched in "cell periphery and plasma membrane" terms but these were not present in the WUGs-GSEA. Instead, MYBF1-GCN and MYB24-GCN were highly enriched in "photosynthesis-related" and "terpene synthase activity" terms, respectively, thus overlapping with the enriched terms found in the variegated WUGs (Fig. 3A). The GCN of MYB24, the only uncharacterized TF from this list, contained several specialized metabolic genes related to phenylpropanoid, benzenoid, and terpenoid compounds and also to phytohormone (e.g. jasmonic acid and gibberellin) and fatty acid metabolic pathway genes. Several functionally characterized genes involved in the synthesis of mono- and sesquiterpenes were present. Among these, a very high correlation was found particularly with TPS35 (VIT_12s0134g00030), an in vitro–characterized monoterpene synthase (Supplemental Data Set 7) (Martin et al. 2010). Our GCN corroborates previous studies showing *MYB24* as coexpressed with terpene synthase (*TPS*) genes (Carbonell-Bejerano et al. 2014; Savoi et al. 2016), but it also suggests a more complex regulatory network composed of light response, phytohormone, and metabolic pathway genes.

MYB24 expression correlates with the transcript accumulation patterns of several members of the *TPS* family

The grape MYB24 (VIT_14s0066g01090; Vitvi14g01750) is the only R2R3-MYB factor belonging to Subgroup 19 (S19) in this species (Wong et al. 2016) and is the closest homolog of Arabidopsis AtMYB24, AtMYB21, and AtMYB57, all of which are highly expressed in inflorescences and promote flower maturation in a developmental regulatory network also involving ARF and bHLH TFs (Cheng et al. 2009; Reeves et al. 2012; Qi et al. 2015). In concordance with its characterized orthologues, *VviMYB24* shows high expression in flowers, increasing toward the late stage of their development (Supplemental Fig. S4A). Additionally, it shows an exponential increase in expression in berry ripening stages toward harvest and postharvest withering. After reanalyzing public transcriptomic data sets, we identified *MYB24* as being highly expressed in berry skins under 2 environmental stress conditions: UV-B (in a pigmented cultivar) (Carbonell-Bejerano et al. 2014) and drought (white-skinned cultivar) (Savoi et al. 2016). Reinspection of RNA-Seq data also allowed us to identify a splicing variant (*MYB24.2*) that retained its large intron 2 (>3 kb), generating a premature stop codon and leading to an incomplete DNA-binding domain protein. It also lacks a putative transactivation domain located in its C-terminal region, originally described by Liu et al. (2009). The similar transcript profiles of both splicing variants show a clear tissue-specific expression, suggesting the presence of *cis*-binding elements in the *MYB24* promoter that could account for its restricted expression in flowers and berries. Indeed, MADS-box and auxin response elements (ARE) are present in the −3kb-to-transcriptional start site (TSS) region. These elements are known to give flower-specific expression in Arabidopsis (Reeves et al. 2012) (Supplemental Fig. S4B and C).

Both condition-independent (all organs) and condition-dependent (flower/fruit) MYB24-centered networks showed closest relationships with *TPS35/09/10/04* (Supplemental Data Set 7). To identify the key developmental stages of flowers and fruits driving the strong correlation between the expression of *MYB24* and terpenoid pathway genes, we first inspected the cv. 'Corvina' expression atlas (Fasoli et al. 2012). Coordinated expression of several *TPS* genes and *MYB24* was most evident in mature flowers and late stages of both berry skin and pulp development (Supplemental Fig. S5). We also conducted RT-qPCR expression analyses in different stages of flower and fruit development in both high and low terpene-accumulating cultivars (cv. 'Gewürztraminer' and 'Viognier', respectively). *MYB*/*TPS* expression levels were higher in cv. 'Gewürztraminer', independently of the stage considered. Among all *TPS* genes surveyed, *MYB24* was tightly coexpressed with *TPS35*, as well as with the sesquiterpene synthase genes *TPS10*, *TPS14*, and *TPS07* in both cultivars. *TPS09* was annotated only in VCost.v3, so it was not possible to find it in the "Corvina" atlas. *MYB24* and *TPS13* expression was correlated only in the high terpene-accumulating cv. 'Gewürztraminer' (Supplemental Fig. S6).

MYB24 binds to a set of TPS genes and flavonol regulators, promoting these pathways in response to anthocyanin depletion in berry skin

As grape MYB homologues seemed abundantly coexpressed with TPSs, we interrogated whether MYB24 could potentially regulate these genes. We performed DNA affinity purification sequencing (DAP-seq) to examine the in vitro binding of affinity-purified MYB24 protein to gDNA in cv. 'Cabernet Sauvignon' (O'Malley et al. 2016). Based on peak calling and motif discovery, MYB24 DAP-seq general statistics were similar to those previously described for Arabidopsis R2R3-MYBs (Bartlett et al. 2017). The number of peaks was quite similar between the 2 phased haplotype references (6,869 and 6,170 for the CS08 primary (p) and p + haplotig contigs, respectively). De novo discovered motifs from sequences under the 600 most enriched peaks were nearly identical for both analyses, showing the core "ACCTAAC" consensus motif (Fig. 4A). This motif is consistent with an AC-element consensus sequence (ACC[A/T]A[A/C][T/C] or ACC[A/T][A/C/T][A/C/T]) previously associated with S19 MYBs in Arabidopsis (Kelemen et al. 2015). The AC-element has also been found in nectary gene promoters (TCACCTAA(C/A)) that are bound by a S19 MYB gene (LxS-MYB305) in ornamental tobacco (*Nicotiana langsdorffii* × *Nicotiana sanderae*) (Liu et al. 2009).

The 6,170 identified binding sites were assigned to their closest gene feature in the CS08 genome, reaching a total of 5,021 bound genes (Supplemental Data Set 9). Peaks were widely distributed throughout upstream, downstream, and inside-gene regions, but a higher proportion was observed close to TSS (Supplemental Fig. S7). From all peaks, we found 33 different regions in close proximity to 22 TPS genes (73% in their upstream regions; Supplemental Data Set 10). *TPS* promoter-preferential binding sites were found to be specific to this S19 member and not, for instance, to Subgroup 6 anthocyanin-promoting MYBs such as *Vitis* MYBA1, A6, and A7 nor to Arabidopsis MYB113 (Fig. 4B; Supplemental Fig. S8). We searched for the identified AC-element in these 22 *TPS* genomic regions, observing an enrichment for a subgroup of *TPS* genes, revealing a preferential binding of MYB24 to *TPS* promoters (Fig. 4C). We remapped the DAP-seq reads in the 12X.2 PN40024 reference genome to ascertain the identity of each *TPS*-bound gene, identifying the MYB24 coexpressed *TPS35/09/10* (GCN; Fig. 4D) and *TPS13* (RT-qPCR) genes. MYB24 also binds within the promoters of 32 photosynthesis or light-related genes and 10 genes related to isoprenoid/carotenoid metabolism (Supplemental Data Set 11), including genes encoding farnesyl diphosphate synthase (FPS), geranylgeranyl pyrophosphate synthetase 1 (GGPPS1), carotenoid isomerase (CRTISO2), *cis*-zeta-carotene isomerase (Z-ISO), 9-*cis*-epoxycarotenoid

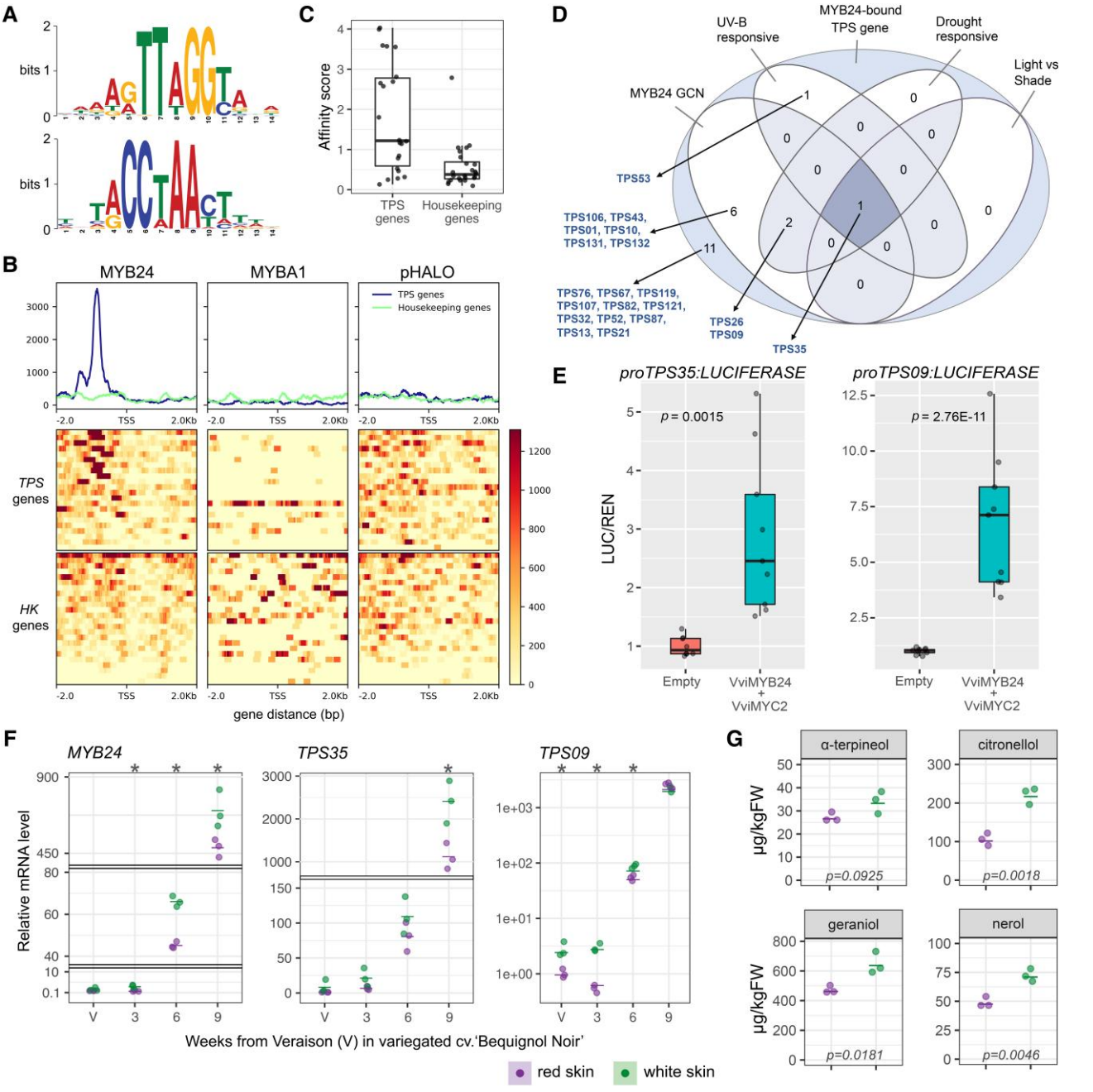

Figure 4. Discovery of genome-wide transcription factor binding sites (TFBSs) by DAP-seq identifies *TPS35* and *TPS09* as HCTs of MYB24. **A)** Binding motif derived from the 600 most significant peaks of MYB24 DAP-seq, in forward (top) and reverse complement (bottom) directions. **B)** Smoothed DAP-seq binding signal at (−2 kb, +2 kb) from the TSS (*x* axis) in 22 *TPS* genes and compared with background housekeeping (HK) genes for MYB24, the anthocyanin regulator MYBA1, and empty vector (pIX-HALO) as a negative control. **C)** Average motif score ("affinity") of the MYB24 binding motif across the entire (−2 kb, +500 bp) region of *TPS* and HK genes. **D)** Intersection of *TPS* genes bound and coexpressed with MYB24 in different transcriptomic data sets (GCN, gene-centered aggregated coexpression network). **E)** Transient expression of *VviMYB24* with *VvibHLH07/MYC2* activates the *VviTPS35* and *VviTPS09* promoters. *Nicotiana benthamiana* plants were agroinfiltrated with 35S:VviMYB24 and 35S:VviMYC2 constructs either alone or in combination (empty vector used as a negative control) and kept in low-light conditions for 3 d before LUC activity quantification. *P* values were calculated based on 1-way ANOVA followed by Tukey's post hoc test. **F)** *MYB24* and target *TPS* gene expression profiles at different ripening stages in red and white skin sections of variegated berries of cv. 'B. Noir'. Sixteen berries from 8 clusters belonging to 5 plants were used for each sample. Gene expression data from 3 biological replicates are shown (averages as horizontal lines). Asterisks indicate significant differences ($P < 0.05$) between tissues based on 1-way ANOVA followed by Tukey's post hoc test (performed independently for each developmental stage). **G)** GC-MS targeted monoterpene quantifications in red and white skin sections of variegated berries of cv. 'B. Noir' at maturity (9WAV). *P* values were calculated based on 1-way ANOVA followed by Tukey's post hoc test. For all boxplots, the lower border and upper border of the box show the lower quartile and upper quartile, respectively. The line in the box shows the median. Whiskers show min to max.

dioxygenase (NCED6), zeaxanthin epoxidase 1 (ZEP1), and lycopene epsilon cyclase (LCYE).

MYB24 is clearly a nucleus-localized transcriptional activator, as shown by MYB24:eGFP localization and Gal4DBD:MYB24 activity assays in agroinfiltrated *Nicotiana benthamiana* cells and yeast, respectively (Supplemental Fig. S9). Thus, in order to establish a list of high-confidence targets (HCTs) among MYB24-bound genes, we overlapped the DAP-seq data (binding up to −5 kb from TSS; Supplemental Data Set 12) with MYB24 coexpression data (networks from Supplemental Data Set 7 that also include MYB24-bound *TPS* genes that contain MYB24 as part of their own GCN; Supplemental Data Set 13) and with reanalyzed transcriptomic data sets from ripening berries where *MYB24* was upregulated, namely in response to UV-B radiation (NimbleGen microarray data; Supplemental Data Set 14) (Carbonell-Bejerano et al. 2014), in light vs shade treatments (Illumina RNA-Seq; Supplemental Data Set 15) (Sun et al. 2017), and in response to water deficit (Illumina RNA-Seq; Supplemental Data Set 16) (Savoi et al. 2016). Three genes were present in all list sets: *TPS35*, a putative jasmonate *O*-methyl transferase gene (*JOMT*), and a zinc knuckle putative transcriptional regulator gene (*ZnKn*). Twelve MYB24-bound genes were present in at least 3 data sets, including a UDP-glycosyl transferase gene of unknown function (*UGT-like1*), a thioesterase gene, and a *S*-adenosyl-L-methionine:salicylic acid carboxyl methyltransferase gene (*SAMT*) (Supplemental Fig. S10 and Data Set 17).

As *VviTPS35* and *VviTPS09* are HCTs, we tested the transcriptional regulation of these genes by VviMYB24 with a dual-luciferase (dual-LUC) assay in *N. benthamiana* agroinfiltrated leaves. Arabidopsis AtMYB24 and AtMYB21, which play a role in flower maturation, must interact with bHLH factors (AtMYC2/5) in order to succeed in these roles (Qi et al. 2015). As expected, the activation of the *VviTPS35* promoter (1.66 kb upstream of the ATG) required coinfiltration with *AtMYC5* (Supplemental Fig. S11). We used AtMYC5's sequence to search for its homologues in grapevine (Toledo-Ortiz et al. 2003), identifying the ubiquitously expressed *VviMYC2* (*VvibHLH007*) as the closest homologue (Supplemental Fig. S12, A and B). The activity of the *VviTPS35/09* promoters was also dependent on the coinfiltration of *VviMYC2* (Fig. 4E). A bimolecular fluorescence complementation (BiFC) assay demonstrated the interaction of VviMYB24 with AtMYC5 and VviMYC2 in *N. benthamiana* agroinfiltrated leaves (Supplemental Fig. S12C).

The binding and reciprocal coexpression observed for several *TPS* genes (Supplemental Fig. S13), together with the direct activation of *TPS35* and *TPS09* by MYB24, implied that terpenes should differentially accumulate whenever *MYB24* increases its expression, i.e. in late flowering and late berry ripening developmental stages, in white skin sections of cv. 'Béquignol' variegated berries and in response to radiation and drought. In fact, this is what we observed; first, high *MYB24*–terpene correlations were found during flower/fruit development in both high and low terpene-producing cultivars (Supplemental Fig. S14). Also, by reanalyzing and integrating the results of 2 metabolomics/transcriptomics studies (Savoi et al. 2016, 2017), we found that *MYB24* expression was highly correlated with the accumulation of berry monoterpenes (geraniol, nerol, linalool, and alpha-terpineol) in response to drought (Supplemental Fig. S15). We further explored this relationship in the variegated samples by dissecting white and red skin sections, quantifying gene expression throughout all ripening stages, and using targeted and untargeted gas chromatography–mass spectrometry (GC-MS) metabolomics at the harvest stage (9WAV). *MYB24*, *TPS35*, and *TPS09* showed very similar expression profiles, with an exponential behavior increasing toward the late stages and increasing their expression in the white skin sections in at least 1 timepoint (Fig. 4F). Among volatile compounds with higher accumulation in white variegated berry skin sections, we identified the monoterpenes citronellol (in both targeted and untargeted assays), geraniol, nerol, and alpha-terpineol (Fig. 4G; Supplemental Fig. S16).

We suggest 418 additional putative MYB24 targets based on the overlap of DAP-seq data with at least 1 of the 4 considered data sets (mapped to the PN40024 12X.2 assembly and associated with its VCost.v3 annotation; Supplemental Data Set 17). In addition to an enriched "terpenoid-related" term, MapMan pathway analysis of these HCTs also showed enrichment of jasmonate-, abscisic acid-, and demethylation-related terms (Supplemental Fig. S17 and Data Set 18). HCTs also include the light-responsive flavonol pathway regulators *HYH* (Loyola et al. 2016) and *MYBF1* (Czemmel et al. 2009) and several photosynthesis-related genes. VviHY5/HYH regulate several early light responses, including flavonol accumulation via activation of the regulator *MYBF1* and metabolic pathway genes such as *FLAVONOL SYNTHASE 1* (*FLS1*) and the flavonol glycosyl transferase genes *GT5/6* (Loyola et al. 2016; Czemmel et al. 2017). MYB24 binds to the *HYH* promoter at around −0.92 kb from the TSS (Fig. 5A) and *MYBF1* at −3.6 kb upstream of the start codon (Supplemental Data Set 12). A dual-LUC assay in *N. benthamiana* agroinfiltrated leaves demonstrated that the activity of the *HYH* promoter (1.53 kb upstream of the ATG) was enhanced by coinfiltration of *VviMYB24* and *VviMYC2* (Fig. 5B). It was not possible to amplify an ∼4 kb promoter to test *MYBF1* activation. However, and as expected, *HYH*, *MYBF1*, and their target *FLS1* and *GT5* were induced in the white skin sections of variegated berries throughout berry ripening, as shown by RT-qPCR (Fig. 5C). Analysis of the flavonol contents of white skin sections quantified at 5WAV showed increased levels of the glycosylated forms of quercetin and kaempferol compared with red skin sections. These flavonol types are known to accumulate in berries in response to UV radiation (Martínez-Lüscher et al. 2014). In particular, the contents of 2 flavonols, quercetin-3-glucoside (q-3-glc) and q-3-glc-6-ac, in the white skin sections of the variegated berries were triple the amount found in pigmented skin samples. Quercetin-3-gal and kaempferol-3-glc were also more abundant in the variegated

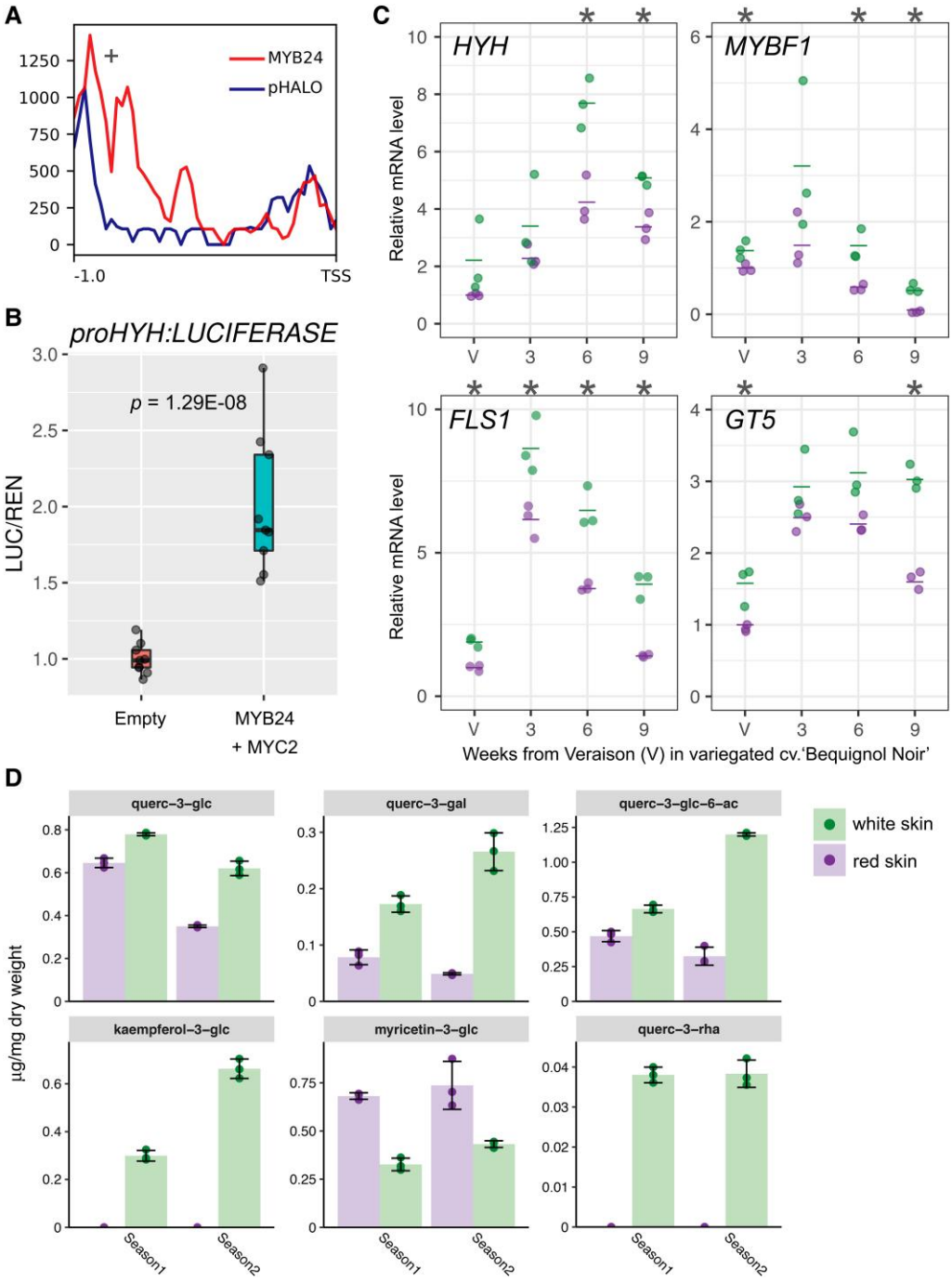

Figure 5. MYB24 promotes flavonol accumulation via the binding and regulation of the flavonol regulator *HYH*. **A)** MYB24 binds to the promoter of the light-early response regulator *HYH*. DAP-seq binding signal (+) at −0.92 kb from the TSS (*x* axis), compared with empty vector (pIX-HALO) as a negative control. **B)** Transient expression of *VviMYB24* with *VvibHLH07/MYC2* activates the *VviHYH* promoter in *N. benthamiana* leaves. *P* values were calculated based on 1-way ANOVA followed by Tukey's post hoc test. **C)** The expression profiles of flavonol-related genes (*HYH*, *MYBF1*, *FLS1*, and *GT5*) at different ripening stages in red and white skin sections of variegated berries of cv. 'B. Noir'. Approximately 16 berries from 8 clusters belonging to 5 plants were used for each biological replicate. Gene expression data from 3 biological replicates are shown (averages are shown as horizontal lines). Asterisks indicate significant differences ($P < 0.05$) between tissues based on 1-way ANOVA followed by Tukey's post hoc test (performed independently for each developmental stage). **D)** Flavonol composition in 'B. Noir' variegated berry skins at 5WAV at 2 consecutive seasons (vintages). HPLC quantifications are expressed as μg/mg of dry weight. Quercetin 3-*O*-(6′′-acetyl-glucoside) and quercetin-3-*O*-rhamnoside are expressed in quercetin-3-*O*-glucoside (querc-3-glc) equivalents. Standard error bars were calculated from 3 biological replicates, sampled as described before.

white skin sections (Fig. 5D). The integration of the 2 previously included drought studies also showed a high correlation of *MYB24* with kaempferol and quercetin glucosides (Supplemental Fig. S15).

Finally, we observed that among the isoprenoid/carotenoid MYB24-bound genes, 7 genes were HCTs, with all of their binding sites within 5 kb from the TSS (Supplemental Data Set 17). Among these genes, we quantified the expression of carotenoid pathway genes, including *CRTISO2*, *LCYE*, *Z-ISO*, and *ZEP1*, and found that all of them were upregulated in white skin sections of variegated berries (Supplemental Fig. S18A and C). Also, the activity of the *CRTISO2* promoter (2 kb upstream of the start codon) was strengthened by the coinfiltration of *VviMYB24* and *VviMYC2* (Supplemental Fig. S18B). Although carotenoids were not quantified in these skins, it is highly probable that *MYB24* upregulation also promotes the accumulation of carotenoids in white variegated skins.

MYB24 expression is modulated by light exposure in a dose-dependent manner

As the absence of MYBA1/A2 is concomitant with higher levels of *MYB24* transcripts in variegated berries, we first hypothesized that *MYB24* expression could be negatively regulated by MYBA1. However, the notion of the direct regulation of anthocyanin-related MYBs from Subgroup 6 (i.e. *MYBA1*, *A7*, and *A6*) was discarded by inspecting our DAP-seq data, as *MYB24* was not found among MYBA-bound genes. MYBA1 could still indirectly repress *MYB24* expression through a still unknown transcriptional repressor, or alternatively, as MYBA1 triggers anthocyanin production, *MYB24* expression could be negatively influenced by the accumulation of these pigments that are known to filter sunlight in plant tissues (Stapleton and Walbot 1994).

MYB24 is highly induced by radiation, as found in the reanalyzed "UV-B responsive" (Carbonell-Bejerano et al. 2014) and "light vs shade" (Sun et al. 2017) transcriptomic data sets. We confirmed that this light-responsiveness occurred throughout most ripening stages by performing RT-qPCR in berry skin samples obtained from light exclusion, UV-B filtering, and UV-B irradiance treatments conducted in cv. 'Cabernet Sauvignon' plants grown in the field and greenhouse (Matus et al. 2009; Loyola et al. 2016; Czemmel et al. 2017). In all cases, light and UV-B positively influenced *MYB24* expression, a response mirrored by *TPS35* (Supplemental Fig. S19). We further explored data obtained from the field experiments (i.e. full light vs shade and full light vs UV filtering) to investigate the potential impact of different light qualities on *MYB24* expression. After scaling the expression data and interpolating using polynomial regression models, we identified both developmental and environmental factors affecting *MYB24* behavior at late ripening stages (Fig. 6, A and B). *MYB24* expression seems to be primarily driven by development (i.e. ripening) and UV-B radiation and to a lesser extent by visible light (Fig. 6B). However, the contribution of both light factors seems to increase toward the latest ripening timepoints.

The light-responsive behavior of *MYB24* drove us to further inspect whether the differential abundance of anthocyanins could influence the response of *MYB24* to light and if this could explain its lower expression in the red skin sections of 'Béquignol' berries. We inspected gene expression levels in response to light at 2 depths within the berry pericarp (i.e. skin and pulp) in the cv. 'Gamay (G)' and its '*teinturier*' (red-flesh) somatic variant cv. 'Gamay Fréaux (GF)', which is characterized by the accumulation of anthocyanins in the flesh/pulp starting at V (Guan et al. 2016). As expected, shade reduced the expression of *MYB24*, *TPS35*, and *HYH* in both tissues in several post-V timepoints surveyed (Fig. 6C; Supplemental Fig. S20). Additionally, we observed an influence of tissue and cultivar, suggesting a positional effect on the expression of *MYB24* that resembles a light dosage response (i.e. inner pulp tissue being less light responsive than skin). This effect was more evident at the late stage (i.e. 4WAV), when *MYB24* displayed its highest expression (Supplemental Fig. S20) and when the contribution of light factors increased (Fig. 6B). Furthermore, when considering the levels of anthocyanins in these samples, we observed a clear negative correlation between *MYB24* expression and the abundance of these pigments at ripening stages when independently analyzing skins and pulps (Fig. 6D), corroborating a known sunscreen effect of anthocyanins. Lower anthocyanin content could also explain a diminished *MYB24* expression in 'GF' compared with 'G'.

Different light shielding properties of anthocyanins and flavonols are in tune with a temporal delay in UV and high light stress protection in white sectors of variegated berries

The expression of *MYB24* in cv. 'Béquignol' and cv. 'G' and its negative correlation with anthocyanins prompted us to explore if different radiation levels were influencing red and white variegated sectors, as white skins do not accumulate anthocyanin sunscreens but do accumulate higher amounts of UV-shielding flavonols. The anthocyanins malvidin and delphinidin glucosides and the flavonols quercetin and kaempferol glucosides largely accumulate in red and white variegated sectors, respectively (Supplemental Fig. S2, Fig. 5D). We thus studied their light transmission properties as a proxy of their capacity to filter harmful radiation (Fig. 7A). Through an optical setup, we compared different light spectra ranging from UV-C (200 to 280 nm), UV-B (280 to 315 nm), UV-A (315 to 400 nm), and visible (400 to 700 nm) to infrared (IR; 780 to 900 nm). Flavonols and anthocyanins were shown to absorb (i.e. filter) a wide fraction of UV and visible light, respectively. Flavonols showed null capacity in filtering visible light, while anthocyanins absorbed UV wavelengths to a lesser extent compared with their own ability to filter visible light (Supplemental Fig. S21).

The clearly distinct optical filtering properties of flavonols and anthocyanins tested here suggest that variegated skins experience different levels of excessive visible and UV light

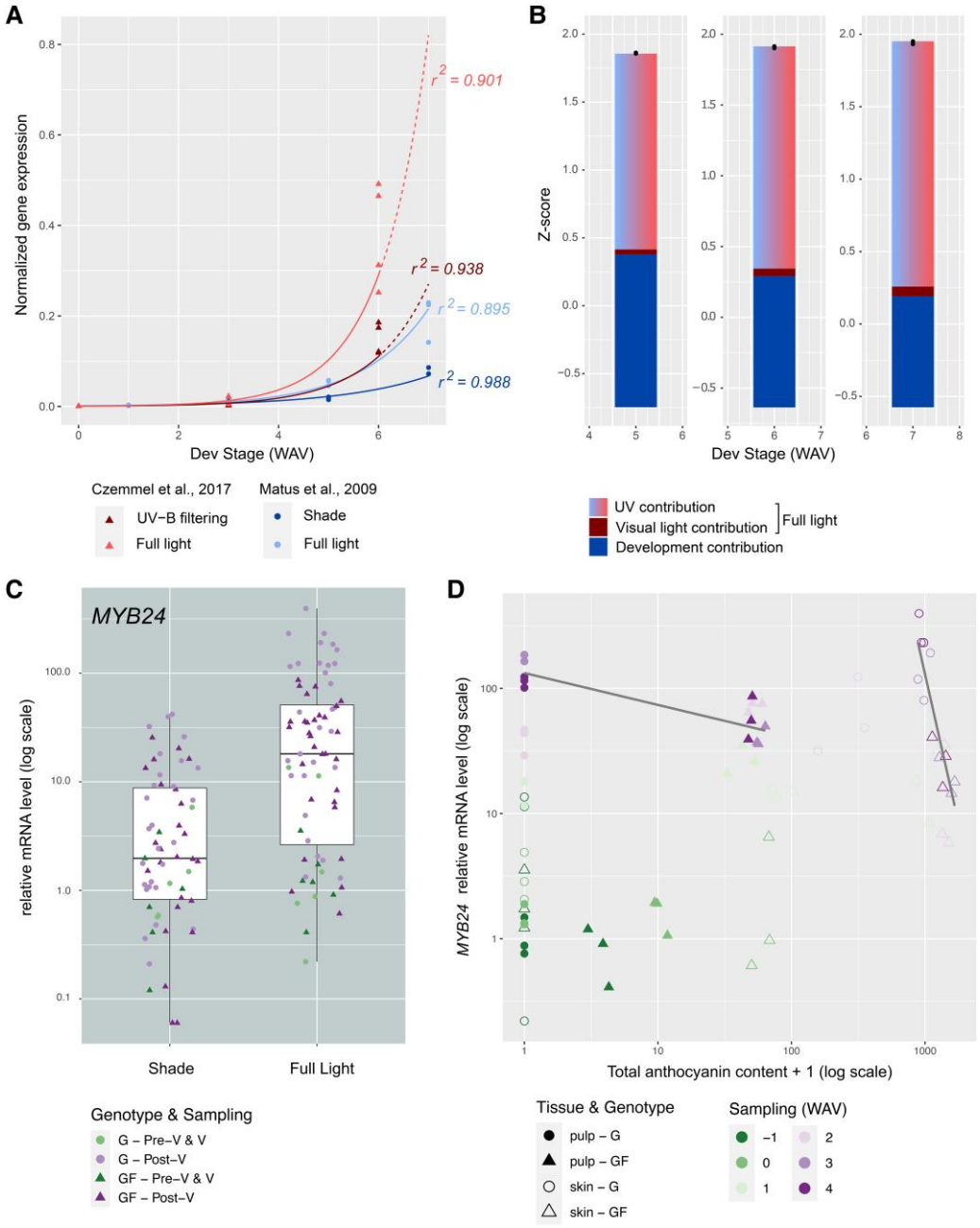

Figure 6. MYB24 responds to different light qualities and is inversely correlated to anthocyanin berry accumulation. **A)** Exponential regression model of *MYB24* expression in full shade (Matus et al. 2009) and UV-B filtering (Loyola et al. 2016) experiments conducted in 'Cabernet Sauvignon' vineyards. Data were independently normalized for each experiment. **B)** Individual contributions of visible light and UV radiation to overall *MYB24* expression during ripening. Normalized z-score values were calculated for each experiment from **A)** and represented at 5WAV and 6WAV (using measured or interpolated values), while predicted values were used for 7WAV (extrapolated using the regression fit curve from **A)**). UV-B contribution is defined as the z-score difference between full light conditions in any of the 2 experiments and the z-score value resulting from UV-B filtering. Visible light contribution is defined as the z-score difference between UV-B filtering and shade values. The developmental contribution is the z-score value of shade at the corresponding timepoint. Black dots depict full light z-score values from both experiments. **C)** and **D)** *MYB24* expression increases during development, but it is negatively influenced by shade, sunscreen (i.e. anthocyanin) accumulation, and berry tissue position. Skin and mesocarp gene expression responses to sunlight exclusion were obtained from field trials of cv. 'G' and its '*teinturier*' (red-flesh) somatic variant cv. 'GF'. Developmental stages: V and pre-/post-veraison (pre-/post-V). A complete fruit sunlight exclusion treatment was imposed by covering grape clusters with opaque boxes (from −2WAV, until maturity) and compared with grape clusters exposed to natural light conditions as a control (100% light incidence).

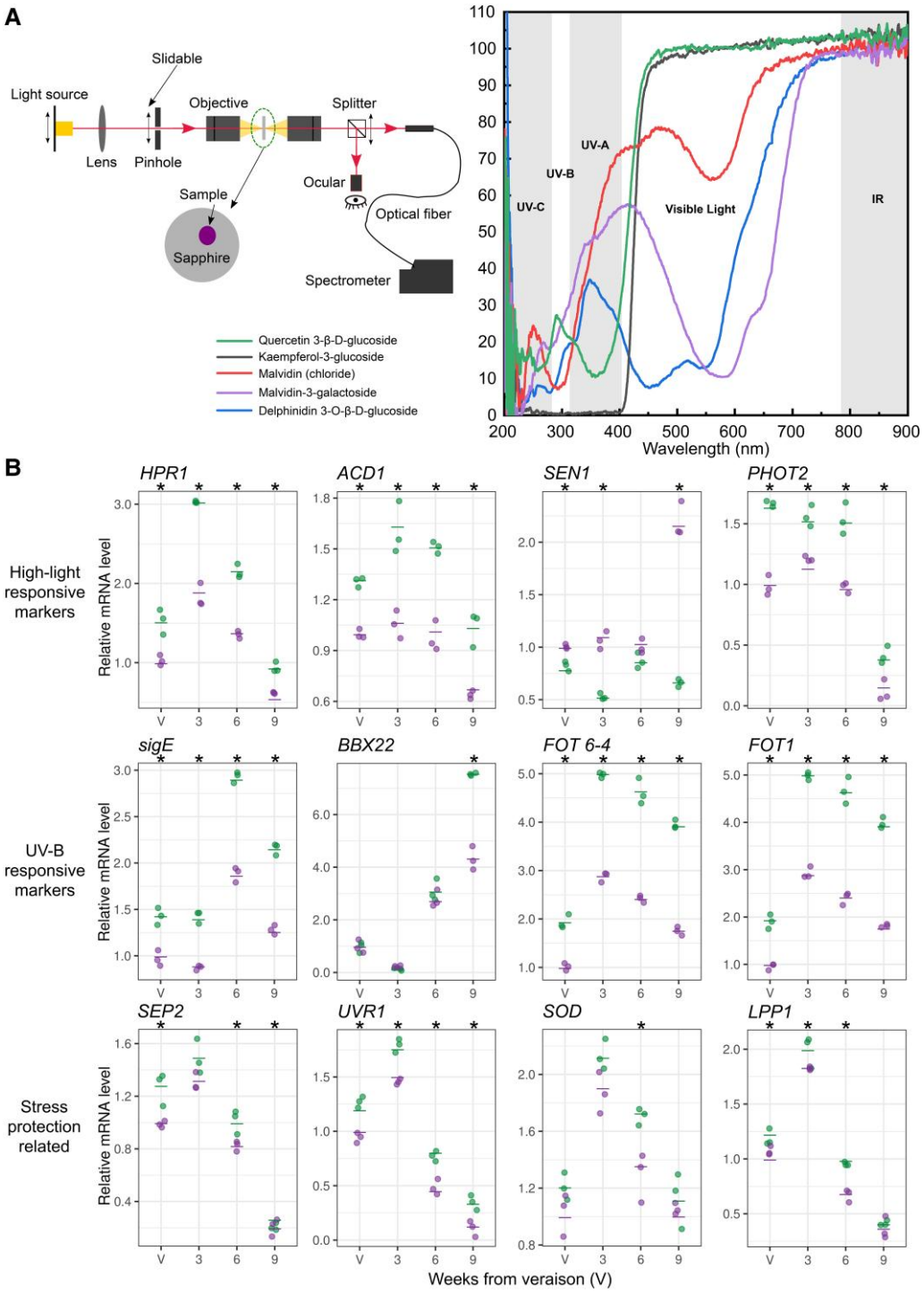

Figure 7. Integration of optical measurements and gene expression profiling shows that white skins of variegated berries are stressed by excessive radiation conditions and that this stress ceases at full maturity. **A)** Differential light shielding properties of berry skin flavonoids. Optical transmittance of common berry skin flavonols and anthocyanins found in white and red skins of cv. 'Béquignol'. Left panel: a home-built optical setup (Liang, Rodríguez, et al. 2022) equipped with a mercury lamp (covering the optical range from 200 to 900 nm), fused silica lenses, and reflecting optics objectives. One drop of each solution was set on top of a sapphire slice that is transparent at the range of 220 nm to 3.5 μm. A visible near-IR spectrometer was used to register light transmittance. Right panel: the optical transmittance spectra of flavonols (quercetin 3-β-D-glucoside and kaempferol-3-glucoside) and anthocyanins (malvidin chloride, malvidin-3-galactoside chloride, and delphinidin 3-*O*-β-D-glucoside chloride). The *x* axis indicates the light wavelengths, classified in UV-C (200 to 280 nm), UV-B (280 to 315 nm), UV-A (315 to 400 nm), visible (400 to 700 nm), and IR (780 to 900 nm) light. The *y* axis shows the percentage of light transmitted through the tested samples. **B)** The relative mRNA levels of light-related genes (high light responsive, UV-B responsive, and light/UV stress protection) at different ripening stages in red and white

(continued)

irradiance depending on the metabolites that accumulate. Based on the *FLS1* gene expression pattern in 'Béquignol' during different stages of development (Fig. 5C) and knowing that flavonols more highly accumulate in white skins (Fig. 5D), we hypothesized that the protective role of these compounds was acquired gradually, reaching a maximum of protection only at very late stages. We thus checked the expression of high light stress–responsive (*HPR1*, *ACD1*, *SEN1*, and *PHOT2*), UV-B-responsive (*sigE*, *BBX22*, *FOT6-4*, and *FOT1*), and stress protection (*SEP2*, *UVR1*, *SOD*, and *LPP1*)–related genes. With the exception of the dark-inducible *SEN1*, which showed the expected increased expression in red skins, all light-related genes were significantly upregulated in white variegated skins (Fig. 7B). This behavior was also observed for MYB24 HCTs *EARLY LIGHT-INDUCIBLE PROTEIN 1* (*ELIP1*), *LIGHT STRESS-RESPONSIVE ONE-HELIX PROTEIN 2* (*OHP2*), and *PHOSPHORIBULOKINASE* (*PRK*), all of which respond to and act in light signaling (Supplemental Figs. S10 and S22; Pastore et al. 2013; Harari-Steinberg et al. 2001; Sharma and Hall 1992). Additionally, most protection-related genes were unresponsive at the latest stage, supporting the notion that even when protective compounds accumulate, the cells in the white skin areas are still stressed at early and middle timepoints and that this stress seems to cease at the end of ripening.

Discussion

Vitis vinifera 'B. Noir' is a red-skinned grape cultivar that produces a rather small proportion of variegated berries with uneven skin pigmentation. This is a stable phenotype that, albeit unreported in the literature, has been observed with persistence over all seasons surveyed in a field collection for at least 67 years. In this study, we show that anthocyanins exclusively accumulate in pigmented skin sections of variegated berries, presenting similar derivative diversity and quantity compared with unvariegated 'B. Noir' berries, as quantified in many other red-skinned cultivars (Castellarin and Di Gaspero 2007).

As largely described for many different grape cultivars and their somatic variants, the depletion of anthocyanins usually results from deletions or mutational-induced inactivation of *MYBA1/A2* TF genes (Ferreira, Pinto-Carnide, et al. 2018). As presented here, the white skins of variegated cv. 'B. Noir' berries showed a genetic configuration resembling that of white cultivars, even though the rest of the plant was hz for *MYBA1/A2* functional alleles. Variegated tissues, as a form of mosaicism, can be described as periclinal or sectorial chimeras. Here, the uneven and "patchy" arrangement of red and white sections we observe in 'Béquignol' variegated berries resembles a "nonpatterned sectorial chimera" where, as described by Frank and Chitwood (2016), it is common to find highly active transposons moving in and out of pigment-related genes, like in the case of the *MYBA1* gene becoming unfunctional due to *Gret1* retrotransposition. This quite rare event differs from the 'B. Gris' periclinal chimera, where 1 cell layer is genetically distinct from the other as a result of mutation propagation throughout the entire layer.

Sectorial chimeras mostly occur due to spontaneous or induced mutations at early stages of embryo development when there is a minimum number of cells in the meristem cell layers. However, the variegated phenotype in 'B. Noir' may arise at different developmental stages and as a mixture of different events, including L2 to L1 displacements and independent mutations occurring at L1 and L2 as cell group–specific *Gret1* retrotransposition events. This would explain the presence of uneven patches together with extended variegated sectors (e.g. covering half a berry).

Cells within a layer tend to move into other layers as cell division proceeds due to errors in the cell division plane (Marcotrigiano 1997). This supports the idea that L2 meristematic cells with unfunctional *MYBA1/A2* alleles would further invade, gradually and heterogeneously, into the epidermal cell layer (L1). This invasion of L1 cells by L2 unpigmented subepidermal cells has been suggested to explain the phenotype of cv. 'Shalistin', from cv. 'Malian' (Walker et al. 2007), and could occur more frequently than the independent mutation in L1 and L2 cells at the same location. Either way, further studies should address the cause of the high transposon instability observed in the 'Béquignol' family compared with other cultivars.

The increased accumulation of flavonols in the white skins of our study subject (Fig. 5D) allowed us to hypothesize that anthocyanin-devoid sections responded more intensely to sunlight. The roles of anthocyanins in radiation filtering and oxidative damage protection have been well-documented in several plant species. In addition, here, we show that grape anthocyanins are capable of filtering both UV and visible light with different capacities, depending on their wavelength (Fig. 7A). Correspondingly, the decrease or complete depletion of anthocyanins in the skin epidermis negates the protective advantages endowed by these pigments acting as sunscreens (Stapleton and Walbot 1994). When these pigments are absent, as in the case of white

Figure 7. (Continued)
skin sections of variegated berries of cv. 'B. Noir'. Gene expression data from 3 biological replicates are shown (averages shown as horizontal lines). Asterisks indicate significant differences ($P < 0.05$) between tissues based on 1-way ANOVA followed by Tukey's post hoc test (performed independently for each developmental stage). Full gene names are as follows: *HPR1* (hydroxypyruvate reductase), *ACD1* (accelerated cell death 1), *SEN1* (dark-inducible 1), *PHOT2* (phototropin-2), *sigE* (RNA polymerase sigma subunit SigE), *BBX22* (zinc finger B-box TF, AtBBX30 homologue), *FOT6-4* (6 to 4 photolyase), *FOT1* (cyclobutane pyrimidine dimer photolyase), SEP2 (stress enhanced protein 2), *UVR1* (UV-B receptor 1), *SOD* (superoxide dismutase [Cu–Zn]), and *LPP1* (lipid phosphate phosphatase 1).

skin sectors of variegated berries, sunscreen-depleted cells respond to ensure alternative mechanisms for light stress protection. In this scenario, epidermal layers of berry skins are sheltered from the effects of excessive light and ultraviolet radiation by accumulating flavonols. This response to excessive light represents 1 of the fastest metabolic responses to environmental light-related stresses ever described in plants (Agati and Tattini 2010), as they also play important roles as antioxidants in photoprotection.

However, the flavonols tested here do not seem to protect cells from high visible light stress, at least via filtering (Fig. 7A). This is corroborated by the induction of high-intensity light (HL) stress genes in white skin sectors, even at the latest timepoints (Fig. 7B). It has been demonstrated that HL-driven signaling leads to massive transcriptome changes in Arabidopsis involving central TFs such as AtBBX30 (Huang et al. 2019), which includes the dynamic regulation of genes encoding photoreceptors and phytochrome-interacting factors and genes associated with phytohormones, photosynthesis, and the phenylpropanoid pathway. Under HL conditions, excess absorbed energy is produced and multiple reactive oxygen species (ROS) accumulate. Plants acclimate and protect themselves from these effects by protecting the photosystem II reaction centers against photodamage and activating antioxidant mechanisms (Apel and Hirt 2004; Goss and Lepetit 2015; Ruban 2016). Other coping mechanisms include variations in the composition of the photosynthetic apparatus (Walters 2005, Schöttler and Tóth 2014) and leaf optics (Knapp and Carter 1998). In the absence of HL stress ameliorating anthocyanins, it is thus logical to think that plants trigger the accumulation of other metabolites (e.g. terpenes, flavonols, and carotenoids) to promote protection. Additionally, the higher expression of UV and stress-related marker genes in the middle ripening stages of cv. 'Béquignol' also suggest that white skin sectors are stressed due to the effects of ultraviolet radiation despite them having already initiated the accumulation of UV-shielding flavonols (Figs. 5D and 7B).

Our results suggest that the accumulation of isoprenoids, in particular monoterpenes, is also triggered by MYB24 in response to higher radiation caused by anthocyanin depletion. The potential roles of monoterpenes in dealing with oxidative stress have been previously suggested, i.e. to directly mitigate ozone levels and scavenge ROS, leading to decreased oxidative damage and improved thermotolerance (Lee et al. 2015; Zuo et al. 2017). Although previous studies in grapevine showed that terpene levels increase in response to radiation (Carbonell-Bejerano et al. 2014; Friedel et al. 2016), less is known about how TPSs are transcriptionally activated by light. We determined that MYB24 is a key regulator of this response. The contents of the monoterpenols terpineol, citronellol, geraniol, and nerol increased significantly in the nonpigmented sections of variegated berries (Fig. 4G). We cannot discard the notion, however, that depending on the cultivar, the accumulation of other terpenes could be regulated by MYB24. Also, we cannot rule out the possibility of a single TPS producing different terpenes in planta, despite being validated in vitro for just 1 specific compound. For instance, cv. 'Gewurztraminer' produces beta-ocimene in high correlation with *TPS35* and *MYB24* expression, while 'Béquignol' does not accumulate this specific compound despite *TPS35* being upregulated. Considering that TPSs have been proven to be promiscuous in many species including grape (e.g. Martin et al. 2004) and that SNPs in a *TPS* gene can lead to different products (Smit et al. 2021), it is possible that TPS35 produces different terpenes depending on the cultivar.

The infrequent variegation phenotype observed in this study provided an ideal framework for studying the genetic control of both flavonoid and isoprenoid metabolism. Our transcriptomics and RT-qPCR gene expression analyses of the variegated berries showed that several genes associated with photosynthesis (including photosystem function), carotenoid metabolism, and UV/light- and stress-induced responses were significantly induced in white skin sections (Figs. 3C and 7B; Supplemental Figs. S18 and S22), in addition to the regulatory and structural pathway genes related to the accumulation of terpenes and flavonols. The activation of these genes upholds the theory that white skins are experiencing increased radiation due to the lack of anthocyanin sunscreens. In an effort to explore how variegated berries may activate terpenoid and flavonol metabolism, due to the uneven distribution of skin anthocyanins during ripening, we searched for gene expression changes in TFs potentially governing these responses. Our transcriptomic/metabolomic meta-analyses, cistrome data, and their validation through several approaches suggested that these changes are governed transcriptionally through the activity of a few TFs from the R2R3-MYB (MYB24 and MYBF1) and bZIP families (HYH).

The inspection of MYB24 HCTs showed an enrichment of the term "secondary (i.e. specialized) metabolism terpenoids" (Supplemental Fig. S17). In addition, the DAP-seq data of MYB24, its expression behavior in terms of light-responsiveness, and its high correlation with the increase in light-responsive gene expression and the accumulation of metabolites in all the data sets generated and reanalyzed (Supplemental Figs. S15 and S19) reveal a major role of this TF in the general light signaling pathway. For instance, MYB24 binds to genes encoding an early light-inducible protein (*ELIP1*), a one-helix protein 2 (*OHP2*), and a phosphoribulokinase (*PRK*), all of which are related to the light stress response (Sharma and Hall 1992; Harari-Steinberg et al. 2001; Pastore et al. 2013) (Supplemental Fig. S22). Gene ontology (GO) analysis of MYB24-bound genes revealed "RNA biosynthesis-Transcriptional regulation" as a highly significant enriched term (Supplemental Fig. S17); in fact, ~7.3% of its target genes encode TFs, placing MYB24 in a top hierarchy of transcriptional regulation.

Among MYB24 targets encoding TFs, we identified *HYH* and *MYBF1*, both encoding TFs associated with light and UV-B radiation responses in grapevine (Loyola et al. 2016;

Czemmel et al. 2017). *HYH* expression seems to be sensitive to the increase in MYB24 levels due to light stress but not much to its increase during development, as *HYH* expression tends to decrease at late ripening. Although we could not demonstrate the MYB24-mediated activation of *MYBF1*, MYB24 could at least indirectly regulate its expression through the induction of *HYH*. HY5 and HYH regulate each other, act as partially redundant central mediators of photomorphogenic responses and are considered to be marker genes of light signaling (Lee et al. 2007; Binkert et al. 2014). Because of their "very early" behavior, we cannot rule out the possibility of feedback regulation of MYB24 by any of these bZIP regulators. As shown here, the control of flavonol accumulation by MYB24 is indirect, i.e. through the activation of HYH and MYBF1 as intermediate regulators. Despite this, it seems to be a stable process, as *MYB24* was previously identified among several metabolic QTLs segregating with flavonol content in ripe berry skins (Costantini et al. 2015). Additionally, *MYB24* and flavonols showed a high correlation in our integrated analysis of 2 drought studies (Savoi et al. 2016, 2017).

Our results suggest that MYB24 potentially regulates an additional metabolic pathway. MYB24 binds in close proximity within the promoters of 10 genes related to isoprenoid/carotenoid metabolism. The clearest role of MYB24 in modulating light responses through carotenoids is observed with the carotenoid isomerase *CRTISO2* and lycopene beta-cyclase *LCYE* genes, which were highly induced in the white skin sections of variegated berries (Supplemental Fig. S18A). CRTISO2 promotes the accumulation of trans-lycopene. LCYE produces alpha-carotene from lycopene and is the first committed step in the production of lutein, the most abundant carotenoid (xanthophyll) in photosynthetic plant tissues where it plays important roles in light-harvesting complex-II structure and function (Kim and DellaPenna 2006; Richaud et al. 2018).

Previous studies have provided evidence for an opposite relationship between terpenes or carotenoids (either the metabolites or their related genes) and anthocyanins, especially when comparing cultivars with different degrees of pigmentation (Cravero et al. 1994; Bunea et al. 2012; Massonnet et al. 2017; Zheng et al. 2021). Our data put MYB24 and its regulatory network in the center of this conjuncture (Fig. 8). Anthocyanin depletion results in excessive radiation leading to UV and high light stress responses in white skin sections, ultimately boosting *MYB24* and *HYH/MYBF1* expression and leading to the accumulation of disubstituted (i.e. quercetin) and monosubstituted (i.e. kaempferol) flavonols. On the contrary, skin-localized anthocyanins seem to produce a self-shade effect over the mesocarp cells, reducing *MYB24* expression in pulp compared with skins (Fig. 5B). The inverse correlation of *MYB24* and *TPS* expression and anthocyanin abundance in berry skin at late stages of ripening is also demonstrated when comparing pink and dark red cultivars (Santibáñez et al. 2019). Our data strongly suggest that high light and a fraction of the nonfiltered UV spectra upregulate *MYB24* expression as a consequence of the lack of epidermal sunscreens. However, we cannot rule out the possibility of indirect repression of *MYB24* by MYBA1 (Fig. 8). In fact, *MYBA1-UFGT1* and *MYB24* also showed a negative correlation in the cv. 'G' study (Supplemental Fig. S23).

Very few TFs are known to control terpene synthesis in model plant species, and even less are known as regulators of more than 1 metabolic pathway. Previous studies have implied that VviMYB24 is related to terpene and flavonol accumulation (Savoi et al. 2016; Lu et al. 2021), while their roles in carotenoid accumulation have been unclear. Our study demonstrates that MYB24 is a key coordinator of these pathways as part of the UV/HL-driven signaling response. All these processes respond to the depletion of the anthocyanin sunscreen in variegated berries, thereby contributing to the opposite abundances between isoprenoids and anthocyanins found in fruits.

Materials and methods

Plant materials and field sampling of grape organs throughout development

Ripening berries belonging to the *V. vinifera* cultivars 'B. Noir' (some with variegated berries) and 'B. Blanc' were sampled from a grapevine germplasm collection (INRA, France) at 5 wks after the onset of ripening/V (5WAV) in 2 consecutive years (for transcriptomic analysis) and every 2/3 wks, starting from V for RT-qPCR gene expression analysis and volatile aroma compound identification and quantification. Approximately 2 berries from 8 clusters belonging to 5 plants were used for each biological replicate ($n = 3$). The berries were immediately frozen in liquid nitrogen, peeled after slight thawing, and deseeded in liquid nitrogen, and the skin and pulp were kept separated for later analyses. The samples were ground into a powder in liquid nitrogen using a ball grinder MM200 (Retsch, Haan, Germany) and stored at −80 °C for later analysis. Grape berries were also harvested from cv. 'Gewürztraminer' (at 40, 53, 67, 84, 101, and 116 d after anthesis, DAA) and cv. 'Viognier' (32, 45, 73, 92, and 105 DAA) vineyards located in Oliver (BC, Canada). Forty berries per sample were collected for terpene and transcript analyses; berries were cut off from the cluster at the pedicel level, snap frozen in liquid nitrogen, and stored at −80 °C. Open flower samples were collected from 2-year-old vines grown in the UBC Horticulture Greenhouse. At each developmental stage, 3 biological replicates per cultivar were performed. All berries were immediately peeled and deseeded before sample storage. All organs and tissues were frozen in liquid nitrogen and stored at −80 °C until required for HPLC or GC analyses or RNA extraction.

Microscopy

Sections of ripening berries (at 5WAV) were generated with a vibrating-blade microtome (Microm HM 650 V). After cutting the fruit in 2 at the equatorial zone with a scalpel, the

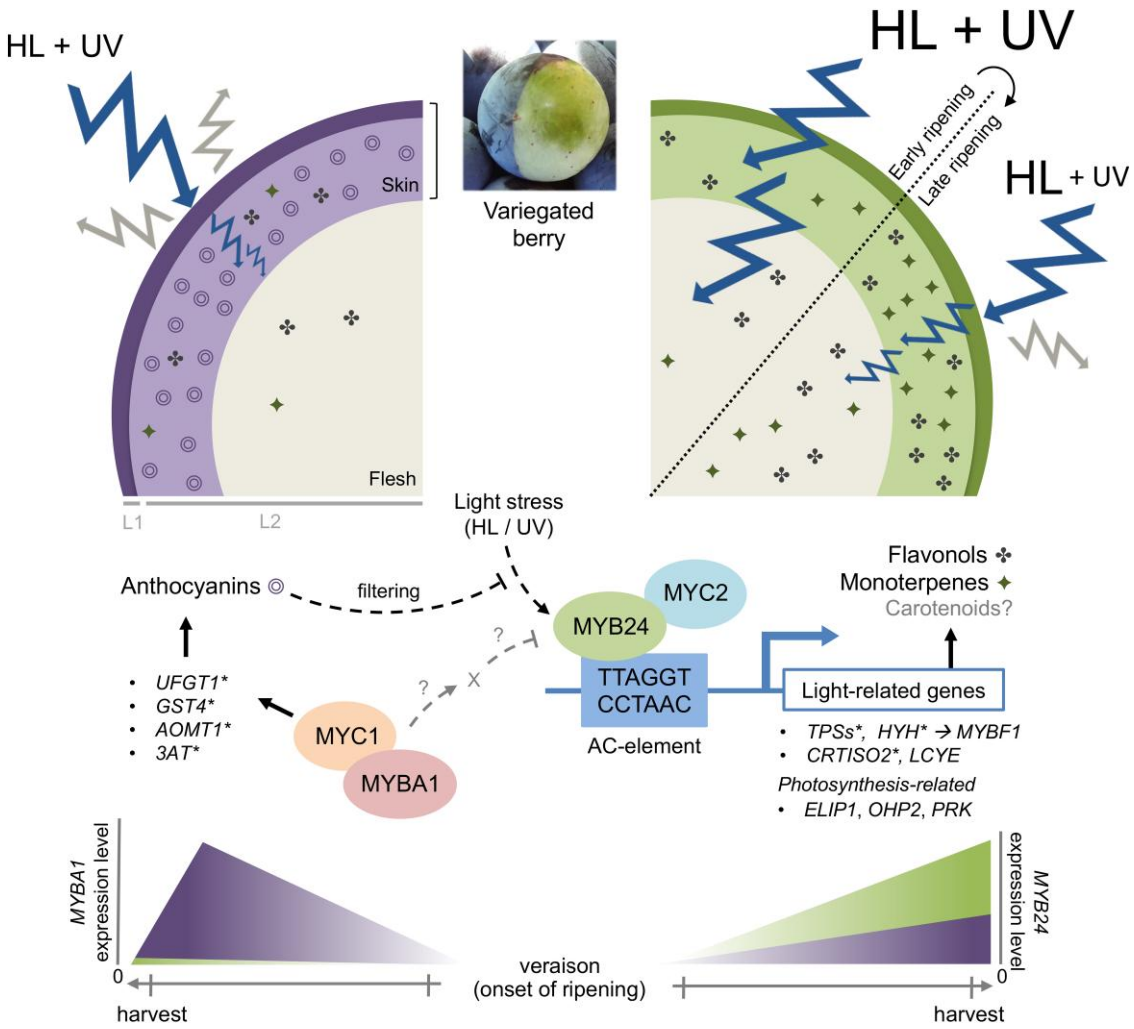

Figure 8. A proposed model for the response of white skin sections of variegated berries coping with HL and UV radiation stress. In red skin sections, the *MYBA1* regulator is expressed, thus activating the production of anthocyanin pigments that prevent damage by filtering excessive radiation. Due to the lack of these intrinsic sunscreens, the white skin sections of variegated berries experience HL and UV stress, resulting in *MYB24* induction. MYB24 regulates light-related processes, including monoterpene and flavonol biosynthesis, by binding to the promoter regions of *TPSs* and regulator genes (*HYH*), respectively. Carotenoid pathway genes are also regulated. The known antioxidant properties of the accumulated monoterpenes and flavonols confer berries a gradual oxidative protection that is maximum at harvest. Alternative specialized metabolic pathways are present in these skins to protect cells from the harmful effects of excessive light stress.

half berry obtained was fixed on a piece of metal placed in the center of a tank-driven microtome. Cross-sections from 60 μm to 100 μm were cut in water and mounted between a slide and a coverslip with a drop of distilled water. Sections were observed at 10× and 20× under a Zeiss Axiophot microscope, and digitalized pictures were obtained with a spot camera (Diagnostic Instruments).

Phenylpropanoid extraction and HPLC

Aliquots of 200 mg of berry skin powder were freeze-dried for 72 h, and the dried powders (~50 mg) were extracted in 1.0 mL methanol containing 0.1% HCL (*v*/*v*). The extracts were filtered through a 0.45 μm polypropylene syringe filter (Pall Gelman Corp., Ann Arbor, MI, USA) for HPLC analysis. Each individual sample was analyzed by HPLC as described (Guan et al. 2016, Rodríguez-Lorenzo et al. 2023). Anthocyanin quantification was performed as described in Dai et al. (2014). Flavonol identification was carried out by MS and NMR spectrometry (MS-NRMS; Hilbert et al. 2015). Quercetin 3-*O*-glucoside, quercetin 3-*O*-galactoside, kaempferol-3-glucoside, and myricetin-3-glucoside standards were obtained from Extrasynthese (Genay, France) and used to generate calibration curves.

Molecular marker analysis

Different organs and tissues representing pure L2 (i.e. root and berry pulp) and mixed L1 plus L2 (i.e. leaves and berry skin) cell ontologies were sampled from cv. 'Béquignol' somatic variants, including skin samples from variegated berries. gDNA was extracted using a slightly modified cetyltrimethylammonium

bromide (CTAB)-based extraction procedure as described previously (Lodhi et al. 1994). The haplotype structure was analyzed using 9 different microsatellite markers across distal arm chromosome 2 and analysis of *VvMybA1* and *VVMybA2* alleles. *VvMybA1* gene polymorphisms were investigated using the primers a and d3, and PCR amplifications were performed as reported (Lijavetzky et al. 2006) using previously described F2 and R1 primers (Azuma et al. 2008). PCR fragments were separated by electrophoresis in 1.5% agarose gel in TBE buffer, stained with ethidium bromide, and photographed under UV light. For the *VvMybA2* gene, 1 point mutation (SNP) related to berry color, *VvMybA2R44* (Walker et al. 2007), was investigated as described (Carrasco et al. 2015) and analyzed by capillary electrophoresis (ABI PRISM 310 Genetic Analyzer, PE Applied Biosystems, California, USA), and data analysis was performed using Peak Scanner Software 2 version 2.0. Microsatellites used were described in different publications: VvNTM1, VvNTM3, VvNTM4, VvNTM5, and VvNTM6 (Fournier-Level et al. 2009), SC8_0146_010 and SC8_0146_010 (Ferreira, Castro, et al. 2018), VMC7G3 (Pellerone et al. 2001), and VVIU20 (Merdinoglu et al. 2005). Amplifications were performed separately for each microsatellite, and size was calculated after capillarity electrophoresis at SECUGEN S.L. (ABI PRISM 310 Genetic Analyzer. PE Applied Biosystems, California, USA). The analysis of all capillarity electrophoresis data was performed using Peak Scanner Software 2 version 2.0.

Transcriptomic exploration of variegation

Microarrays were produced using the *V. vinifera* Array-Ready Oligo Set version 1 (Operon Biotechnologies, Germany) as described (Camps et al. 2010). Microarrays were scanned using a GenePix 4000B fluorescence reader using GenePix Pro version 4 image acquisition software (Axon Instruments, Canada). Spot quantification and quality control were done using Maia version 2.75 (Novikov and Barillot 2007). Bad quality spots and those with intensities above 50,000 were filtered before further analyses. Data analyses were performed using the R/Bioconductor (Gentleman et al. 2004) package limma (Smyth 2004). Background correction was done using the normexp method (Ritchie et al. 2007). Array normalization was carried out using the limma function "normalizeWithinArrays" (Smyth and Speed 2003) and the method "printtiploess". *P* value adjustment was done using the Benjamin–Hochberg method. Genes with expression ratio above 1.6 and adjusted (adj) *P* value below 0.1 were considered to be DE. For probe mapping, oligonucleotide probes were mapped to the 12X.1 CRIBI V1 annotation of the PN40024 grapevine genome (Jaillon et al. 2007) as in Ensemble Genes (Kersey et al. 2014) release 22. Best matches were considered to be targets. Genome sequences were annotated using best BLAST matches against the uniref100 database, release 15.14 (Suzek et al. 2007), using the qualifiers: homologous to (>50% alignment identity), similar to (>70%), weakly similar to (≤70%), complete (>98% hit coverage), and partial (≤98% hit coverage). Functional analyses were done using the MapMan and GSEA Ontology (Thimm et al. 2004; Subramanian et al. 2005) and grapevine mappings made for the microarray employed (Rotter et al. 2009). Significantly affected categories were identified using a Wilcoxon rank-sum test implemented in R (R Development Core Team, 2014). Most significantly affected categories were illustrated using R/Lattice.

GCNs

Two distinct aggregate GCNs—condition-independent and condition-dependent GCNs—were constructed from RNA-Seq data sets downloaded from the SRA database. The condition-dependent network only contained data sets extracted from berry tissue from *V. vinifera*, while the condition-independent network contained all available *V. vinifera* data sets. Networks were constructed as described in Orduña et al. (2022). Briefly, the results of 131 and 67 SRA studies were obtained, encompassing 2,766 and 1,615 runs from condition-independent and condition-dependent (berry) samples, respectively (Supplemental Data Sets 19 and 20). Each SRA study was individually analyzed to build a highest reciprocal rank (HRR) matrix (Mutwil et al. 2011). To construct the aggregate whole genome coexpression network, the frequency of coexpression interaction(s) across individual HRR matrices was used as edge weights, and after ranking in descending order, the top 420 frequency values for each gene were chosen to build the final aggregate networks. The list of top 420 most highly coexpressed genes (1% of all VCost.v3 gene models) was used to generate individual GCNs. The individual *TPSs* and *MYB24* GCNs extracted from the condition-dependent and condition-independent networks were analyzed to generate Supplemental Fig. S13.

Reanalysis of public RNA-Seq data sets

Raw sequencing transcriptome data sets were processed using Trimmomatic, and filtered reads were aligned to the aligned to the 12X grapevine reference genome using HISAT2 as previously described (Vannozzi et al. 2018). Expression of grapevine *MYB24* splice variants (*MYB24.1* and *MYB24.2*) was estimated from HISAT2-aligned BAM outputs using StringTie with default settings. Transcript abundance is expressed as transcripts per kilobase million (TPM).

Transactivation assay in yeast

The coding sequence of MYB24 was cloned into the pDEST32 vector by LR recombination to obtain the *Gal4DBD:VviMYB24* construct. The fusion protein vector was transformed into yeast (*Saccharomyces cerevisiae*) strains SFY526 (Wade Harper et al. 1993) and NLY2:SS-38 (Arnerić et al. 2002). Transformants were selected on SD-glucose medium supplemented with -Leu drop-out solution (BD Biosciences). Confirmation of interaction was performed by targeted transformation of the specific constructs using the small-scale yeast transformation protocol as described in the yeast protocol handbook (Clontech). Transformants

were grown in YPDA medium to OD_{600} 0.5 to 0.8. Tubes with 1.5 mL of culture medium were centrifuged at 1,400 rpm for 30 s and the supernant was discarded. The pellet was resuspended by pipetting in 300 μL of Z-buffer. The solution was frozen in liquid nitrogen and thawed at 37 °C for 30 s; this process was repeated 3 times. Finally, transcriptional activity was measured using ortho-nitrophenyl-β-galactoside (ONPG) as substrate for β-galactosidase enzyme released from yeast strains SFY526 and NLY2:SS-38 transformed with *Gal4DBD:VviMYB24*. When hydrolyzed, ONPG generates a galactose molecule and an o-nitrophenol molecule, with the latter being quantified using a spectrophotometer at a wavelength of 410 nm.

Confocal microscopy

Agrobacterium tumefaciens strain GV3101, previously transformed with the vector pK7FWG2 (35S:VviMYB24-eGFP), was grown in 10 mL of liquid LB supplemented with rifampicin 50 ng/L, gentamicin 25 ng/L, and spectinomycin 50 ng/L. Bacteria isolated from the selection medium were resuspended in 4 mL of 10 mM $MgCl_2$ for infiltration. *Nicotiana benthamiana* leaves were infiltrated through the abaxial surface with a needleless syringe. The plants were left in the greenhouse for 3 d. Thirty minutes prior to visualization, 1 cm^2 leaf sections were incubated in a 20 mg/mL solution of 4′,6-diamino-2-phenylindole (DAPI). Fluorescence was visualized under a Nikon Confocal Eclipse C2si microscope. A 405 nm laser was used to excite DAPI, and a filter cube with emission at 445/35 (427 to 462 nm) was used for its detection. For GFP, a 488 nm laser and a filter cube with emission at 525/50 (500 to 550 nm) and 600/50 (575 to 625 nm) were used.

DAP-seq

gDNA was purified from young grapevine leaves of cv. 'Cabernet Sauvignon' CS08 by crude nuclei isolation (with PVP40) and 20% Sarkosyl-chloroform extraction (Thomas et al. 1993). gDNA library and DAP-seq were performed following a published protocol (Bartlett et al. 2017). Briefly, the gDNA sample was sonicated into 200 bp fragments on a Covaris Focus-ultrasonicator instrument, which underwent end repair, A-tailing, and adapter ligation to attach Illumina-compatible sequencing adapters to the DAP-seq library. We verified successful adapter ligation by RT-qPCR of the DAP-seq library with primer sequences that anneal to the adapter, as well as gel electrophoresis of the sonicated gDNA and the DAP-seq library (Bartlett et al. 2017). *MYB24*, *MYBA1*, *MYBA6*, and *MYBA7* were amplified from cv. 'Cabernet Sauvignon' and cloned into the pIX-HALO expression plasmid (TAIR Vector:6530264275) to create an expression vector that contained a HaloTag in frame at the N-terminus. *MYB113* amplified from Arabidopsis was also used (O'Malley et al. 2016).

Clones were verified by digestion with restriction enzyme XhoI. The MYB expression vectors were used in a coupled transcription/translation system (Promega) to produce MYB proteins with the HaloTag fusions. Expression of MYB24 was confirmed by immunoblotting using an anti-HaloTag antibody (Promega). The protein expression reaction was mixed with HaloTag ligand–conjugated magnetic beads (Promega) to pull down the HaloTag-fused TF. The pulled down TF was then mixed with the DAP-seq library in order for TF–DNA binding to occur. A 400 ng library was used in each DAP-seq reaction. The bound DNA was then eluted and PCR amplified to generate sequencing libraries, which were sequenced on an Illumina NextSeq 500 platform (sequencing of libraries was set at 30 million and 1 × 75 bp single-end reads). As a negative control, we performed a DAP-seq experiment with the pIX-HALO expression vector without any ORF insert, accounting for possible nonspecific DNA binding in the reaction mixture, as well as copy number variations at specific genomic loci. Sequencing reads were mapped to the CS08 (140X) and the reference PN40024 (12X.2) genome assemblies available at https://cantulab.github.io/. Enrichment of binding events was first evaluated by plotting genome coverage compared with the negative control (Bartlett et al. 2017). To identify "peaks," enriched regions relative to the control that correspond to binding events, the GEM peak caller was used (Guo et al. 2012), which performs simultaneous peak calling and motif refinement. De novo motif discovery was performed using 200 bp sequences centered at GEM-identified binding events for the 600 most enriched peaks (Bailey et al. 2009). MYB24 target genes were identified by associating the peak regions to the TSS of the closet genes.

Analyzing the overlap of DAP-seq and transcriptomic data sets

DAP-seq peaks were converted from cv. 'Cabernet Sauvignon' to their corresponding cv. 'Pinot Noir' IDs after filtering a BLAST output between both genome annotations (98% identity and 98% coverage thresholds). *TPS* genes were manually curated and assigned to its cultivar counterpart based on BLAST and global alignments. Berry skin transcriptomic data sets from UV-B-irradiated (RMA-normalized) samples (Carbonell-Bejerano et al. 2014) were analyzed using PN40024 12X.2 Assembly V1 annotation, and those of drought-stressed (raw data downloaded from PRJNA313234 BioProject at SRA) (Savoi et al. 2016) and "light vs shade" treatments (raw data downloaded from PRJNA661034 at SRA) (Sun et al. 2017) were reanalyzed using PN40024 12X.2 Assembly VCost.v3 annotation. The RMA-normalized microarray data, containing 2 developmental stages (23° and 26° Brix degrees) and 2 UV-B conditions, were compared using a 1-factor ANOVA (limma package in R). Genes with (adj P value < 0.05 for RNA-Seq data, < 0.1 for microarray data, and logFC > 0.53) in at least 1 berry density were considered to be DE. The Illumina raw sequence reads were trimmed using fastp version 2.0 (the minimum PHRED score accepted for trimming was 20, and reads shorter than 40 bp were discarded). Reads were aligned against the reference PN40024 12X.2 genome assembly using the HISAT2

v2.1.0 aligner with default parameters. Aligned reads were counted with Feature Counts, using the Vcost annotation mapped in 12X.2. Finally, drought and "light vs shade" DE genes (adj P value < 0.05 and logFC > 0.53) were extracted using the limma R package. The overlap between UV-B, drought, and "light vs shade" DE genes, the MYB24-GCN, and the DAP-seq peaks was analyzed using the UpSetplot package in R.

Transient leaf transfection and dual-LUC reporter assay

The transactivation of the upstream regions of *TPS35/09*, *HYH*, and *CRTISO2* by MYB24 was tested using a Dual-Luciferase Reporter Assay (Promega). The promoters/5′ UTRs of *TPS35/09*, *HYH*, and *CRTISO2* from "Cabernet Sauvignon" and the coding sequences of the TF genes *VviMYB24*, *AtMYC5*, *VviMYC2*, *VviMYBA1*, and *VviMYC1* were amplified and cloned into the entry vector pENTR/D-TOPO (Invitrogen) and then transferred by site-specific recombination into the reporter and effector vectors (pPGWL7.0 and pK7WG2.0, respectively) using LR Clonase. The resulting constructs and the reference vector expressing the Renilla luciferase gene (Cavallini et al. 2015) were transferred to *A. tumefaciens* strain EHA105 by heat shock. Dual-LUC assays were performed in Agrobacterium-infiltrated *N. benthamiana* leaves as described in Espley et al. (2009). The combinations of *VviMYBA1* and *VviMYC1* with the *TPS35/09*, *HYH*, and *CRTISO2* promoters were used as negative controls (Supplemental Figs. S18 and S24). Plants were grown from seeds in a greenhouse with temperature between 30 °C and 21 °C, relative humidity of ∼32% to 50%, and 15 h/9 h light/dark cycle, also after agroinfiltration (3 d). Light was given by LED bulbs (Phillips GP LED production DR/B 150 LB), each 1 providing a typical photon flux of 210 μmol/s, consuming 32 W with an efficacy of 3.3 μmol/J. Plants were placed 70 cm below the light source receiving an average of 2,000 lux, measured using a luminometer (MT-912 Light Meter). Firefly (LUC) and Renilla (REN) luminescence were detected using a GENios Pro TECAN instrument. Statistical analysis of the results of the dual-LUC assay is provided in Supplemental Data Set 21.

BiFC assay

The BiFC assays were performed in Agrobacterium-infiltrated *N. benthamiana* leaves as described in Navarro et al. (2020). Four TF genes (*VviMYB24*, *AtMYC5*, *VviMYC2*, and *VviMYC1*) were amplified and cloned to 2 binary vectors (35S:NtGFP and 35S:CtGFP). The recombinant constructs were transferred to *A. tumefaciens* strain C58 by heat shock. A single PCR-positive Agrobacterium transformant was inoculated in medium and grown overnight with the corresponding antibiotics. The final culture was centrifuged at room temperature at low speed (4,000 rpm). The pellets were resuspended in infiltration solution (0.1 M pH = 5.6 2-(N-morpholino) ethanesulfonic acid [MES], 1 M $MgCl_2$). According to each combination, bacteria suspensions were diluted and mixed, keeping the OD600 at 0.2 for each construct. The mixture was infiltrated into the abaxial sides of leaves. Plants were grown and kept in the same light conditions (16 h light/25 °C and 8 h dark/22 °C). After 48 h, infiltrated samples without leaf veins were collected. Samples were observed under a Zeiss LSM780 AxioObserver confocal microscope at 40×. GFP (Exc 488 nm, emission 490 to 544 nm) and chlorophyll (Exc 488 nm, emission 680 to 760 nm) channels were used for visualization.

Nucleic acid extraction and quantification of gene expression by RT-qPCR

Different methods of RNA extraction were used depending on the plant materials. Total RNA was isolated from cv. 'Cabernet Sauvignon' and cv. 'Béquignol' berry skins as described previously (Reid et al. 2006). For cv. 'Gewürztraminer' and cv. 'Viognier', frozen samples were ground to a fine powder in liquid nitrogen using an analytical mill (A11 Basic, IKA). RNA extraction and determination of RNA quality and quantity were performed as described (Wong et al. 2016). The RT reactions were performed with 2 μg of total RNA, reverse transcribed with oligo(dT)15 in a 20 μL reaction mixture using Moloney murine leukemia virus reverse transcriptase (Promega) or a RevertAid First Strand cDNA Synthesis Kit (Thermo Scientific), according to the manufacturer's instructions. RT-qPCR was performed for all genes of interest using specific primers. For cv. 'Béquignol' samples, a Brilliant SYBR Green QPCR Master Reagent Kit (Stratagene) and the Mx3000P detection system (Stratagene) were used. In the remaining cases, PowerUp SYBR Green Master Mix (Thermo Scientific) was used with an ABI 7500 Real-Time PCR System (Applied Biosystems). Amplification of the *UBIQUITIN1* gene (99 bp; Downey et al. 2003), *ELONGATION FACTOR1* (*EF1*; 91 bp), and *ACTIN* (81 bp) (Hichri et al. 2010) was used for normalization of relative gene expression. All RT-qPCR biological replicates were run in 2 or 3 technical replicates within the same plate. PCR conditions, standard quantification curves for each gene, and relative gene expression calculations were conducted as in Wong et al. (2016). Statistical analysis of the RT-qPCR results is provided in Supplemental Data Set 21. Primers are shown in Supplemental Data Set 22.

Analysis of volatiles in cv. 'Gewurztraminer' and 'Viognier'

Free (nonglycosylated) volatile organic compounds (VOCs) were analyzed with some modifications (Kovalenko et al. 2021). Five grams of frozen grape powder were weighted in a 20-mL solid-phase microextraction (SPME) glass screw cap vial with 1.5 g sodium chloride. Then, 4 mL citrate phosphate buffer (pH 5.0) and 100 μL 200 g/L ascorbic acid were added. Finally, 3-octanol (10 ppb final concentration) and d3-linalool (10 ppb final concentration) were added to the sample as internal standards. The free volatile compounds

were extracted and analyzed by headspace–SPME GC-MS. A carboxen–divinylbenzene–polydimethylsiloxane SPME fiber was used (No. 57329-U Supelco, Sigma, St Louis, MO, USA). VOC analyses were performed on a gas chromatograph (model 7890A, Agilent, Waldbron, Germany) equipped with a 5975C mass spectrometer detector and GC PAL80 autosampler (Agilent Technologies). The column used was an Agilent J&W Scientific DB-WAX (30 m × 0.25 mm ID with 0.25 μm film thickness) with a film thickness of 0.25 mm. Helium was used as the carrier gas at a constant flow of 0.8 mL/min. The capped vials were heated at 40°C for 20 min to promote the transference of the compounds from the sample to the headspace. After this step, the SPME fiber was inserted into the sample vial headspace (22 mm depth) for a 30 min sample extraction at 40°C and then inserted into the GC injection port at 250°C and kept for 5 min for desorption. The injection port was lined with a 0.75-mm splitless glass liner. The pulsed splitless injection mode was used. The oven temperature program was as follows: 40°C for 4 min, followed by 3°C/min up to 150°C, 25°C/min to 230°C, and 230°C for 10 min. The mass spectrometer was operated in the electron impact mode at 70 eV, scanning from 33 m/z to 500 m/z. The ion source temperature was 230°C and the quadrupole temperature was 150°C. Data processing was carried out by MSD Chemstation (E.02.02.1431, Agilent Technologies Inc.). Only VOC peaks with signal-to-noise ratios >10:1 were considered for data quantification.

The authentic standards used for identification were reported in Kovalenko et al. (2021). Terpenes were identified by comparing the retention times of ion extracted chromatogram (IEC) peaks, with the retention times of their reference standards when available. The retention indexes (RI) were calculated in relation to a mixture of C7–C30 n-alkanes and compared with published work and by identifying the mass spectra using the Wiley09Nist08 Database (NIST library) (Kovalenko et al. 2021). The volatile concentration of samples was determined based on the calibration curve of the respective authentic standard. Compounds were semiquantified using the calibration curve of the compound with the closest chemical functionality and structure when authentic standards were not available.

GC-MS analysis of volatiles in cv. 'Béquignol' samples

Samples were prepared and solid-phase extracted (SPE). Three biological replicates of red and white skins of variegated berries were used. Skins were ground in liquid nitrogen and suspended in 4 mL of sodium sulfite solution at (Na_2SO_3, 10 g/L). The supernatant obtained after a 15 min centrifugation (11,400 × *g* at 4 °C) was passed through a glass fiber prefilter and a glass filter. Twenty microliters of a 1 g/L 3-octanol solution were added as external standard to allow for the quantification of the major terpenols. The filtrate was passed through a 1 g phase C18 silica-bonded nonpolar column (HF Mega Bond Bond Elut C18, Agilent, 5301 Stevens Creek Blvd, Santa Clara, CA 95051, USA), previously rinsed with 6 mL of methanol and 2 × 6 mL of ultrapure water, at a rate of ~1 drop/s. Total fractions of free and bound monoterpenols were eluted with 4 mL of absolute ethanol. This total terpenol extract was diluted in 40 mL of citrate phosphate buffer (pH 4.5), and the resulting solution was incubated with 50 mg of Rapidase AR 2000 glycolytic enzyme (DSM Food Specialties Beverage Ingredients P.O. Box 1, 2600 MA Delft, The Netherlands) overnight at 37.5 °C to release the glycosidically bound terpenols. The released terpenols were separated by SPE again on a C18 column and eluted with 4 mL of dichloromethane after rinsing with water. Extracts were dried in Pasteur pipettes filled with 0.5 g of anhydrous sodium sulfite and concentrated to 500 μL under a gentle nitrogen flux. Twenty microliters of a 1 g/L m-cresol solution were added to each sample as internal control. Samples were stored at −20 °C prior to GC analysis.

For GC-MS nontargeted analysis, chromatogram files were deconvoluted and converted to ELU format using AMDIS Mass Spectrometry software (http://www.amdis.net), with the resolution and sensitivity set to medium. Chromatograms were then aligned and integrated using SpectConnect (http://spectconnect.mit.edu). All metabolites found in the blank run or believed to have originated from the column bleeding were removed from analysis at this time. After removing contaminant metabolites (volatiles), the IS matrix from SpectConnect was normalized according to the sample weight and 3-octanol surface (external standard). Volatiles were identified by comparing to the NIST 14 standard reference database. Identities of metabolites of interest were then confirmed using authentic standards when available.

Terpenols were quantified by GC-MS targeted analysis. Extracts were analyzed by GC-MS using an Agilent 6890 gas chromatograph equipped with a Gerstel MP2 autosampler and an Agilent 5973N mass spectrometer for peak detection and compound identification. The GC was fitted with a DB-Wax column (30m × 0.32 mm i.d., 0.5 μm film thickness, Agilent J&W, Agilent Technologies France, 3, Avenue du Canada, 91978 les Ulis France). Helium was used as the carrier gas with a column flow rate of 1.5 mL/min. The GC oven temperature was programmed from 45 °C to 235° C, at 2.7 °C/min (hold 10 min). The injector was set to 230 °C and used in pulsed splitless mode (15 psi for 0.50 min). The MS transfer line and ion source temperatures were set at 270 °C and 230 °C, respectively. The MS was operated in EI mode, and positive ions at 70 eV were recorded with a scan range from 30 m/z to 400 m/z. Agilent MSD ChemStation software (G1701DA, Rev D.03.00) was used for instrument control and data acquisition. Injection of a solution of n-alkane standards (C7 C35) was also run to calculate linear RI. Total amounts of alpha-terpineol, citronellol, linalool, nerol, and geraniol were determined using linear calibration curves generated from 5 different concentrations over a range of 0.5 to 100 ng/μL analyzed in triplicate for each standard. Final concentrations were expressed in microgram/kg of fresh weight. Statistical analysis is provided in Supplemental Data Set 21.

Sunlight/UV-B experiments

Three different sunlight or UV-B radiation experiments were conducted using cv. 'Cabernet Sauvignon' commercial plants (either treated in the field or uprooted and transferred to a greenhouse). Experiment 1: low fluence UV-B exposure treatment applied to clusters from 9-year-old potted vines in a UV-free greenhouse during the 2011 to 2012 and 2012 to 2013 growing seasons ($n = 3$), respectively (Loyola et al. 2016). Experiment 2: a UV-B filtering radiation treatment was applied in a commercial vineyard as described previously (Czemmel et al. 2017) during the 2011 to 2012 growing season ($n = 4$). The filtering treatment consisted of blocking solar UV-B radiation by installing a 100 μm clear polyester film at the positions of grape clusters. Experiment 3: sunlight reduction treatments were conducted in the field as described previously (Matus et al. 2009) and consisted of full shading of fruits by the plant's own canopy (0% exposure) and full sunlight exposure from V onwards, generated by displacement of leaves around the cluster region (100% exposure, $n = 3$). Berry skins were frozen in liquid nitrogen and stored at −80 °C until RNA extraction.

Light shading experiments in cv. 'G' and cv. 'GF'

Light exclusion was conducted using 23-year-old spur pruned vines, with a density of 1.6 m between rows and 1 m between plants in a germplasm collection vineyard. Eighteen vines were chosen to form 3 blocks with 3 vines each, and 2 similar clusters from 2 adjacent shoots of each vine were tagged. Opaque boxes were applied to 1 of the 2 tagged clusters of each vine from 2 wks before V until maturity for light exclusion treatment, and the other clusters were exposed under natural light conditions as the control as described previously (Guan et al. 2016). Light-exposed or shaded clusters of both cultivars were sampled weekly from 1 wk after treatment until maturity. Three berries from each cluster and 3 clusters from 3 vines per block were sampled for each treatment at each sampling date. Berries were weighed, deseeded, and separated into skin and pulp, and the skin and pulp were immediately frozen in liquid nitrogen. The samples were ground into a powder in liquid nitrogen using a ball grinder MM200 (Retsch, Haan, Germany) and stored at −80 °C for later analysis.

Correlation of *MYB24/HYH* expression with metabolite composition in berry skins of drought-stressed plants

Transcriptomic data (Savoi et al. 2016, 2017) were remapped to the PN40024 12X.2 assembly and VCost.v3 annotation. Genes with low expression levels were filtered according to the method described in Chen et al. (2016), and raw counts were normalized to fragments per kilobase million (FPKM) values. Applying the WGCN (weighted correlation network analysis) R package (Langfelder and Horvath 2008), the genes were grouped into different clusters. The parameters used were a blockwiseModules with a soft-threshold power value of 30 (fitting a scale-free topology network), a deepSplit of 4, and a mergeCutHeight of 0.2, obtaining a total of 28 modules. The correlation between gene or the modules eigengenes (1st principal component) and metabolite quantification was visualized using the pheatmap (https://CRAN.R-project.org/package=pheatmap) R package, performing a hierarchical clustering using the complete linkage method with Euclidean distance.

Transmission and absorbance analysis of major flavonols and anthocyanins in berries

The optical absorption and transmittance spectra of flavonols (quercetin 3-β-D-glucoside and kaempferol-3-glucoside) and anthocyanins (malvidin chloride, malvidin-3-galactoside chloride, and delphinidin 3-*O*-β-D-glucoside chloride) were measured in a home-built optical setup, described in Liang, Rodríguez, et al. (2022), and consisting of a mercury lamp (covering the optical range of 200 to 900 nm), fused silica lenses, reflecting optics objectives, and a visible near-IR spectrometer (Ocean Optics Maya2000 Pro). The light was spotted using a 20-μm-diameter pinhole. HPLC analytical standards of flavonols (quercetin 3-β-D-glucoside from Sigma-Aldrich and kaempferol-3-glucoside from HWI group) and anthocyanins (malvidin chloride from Cayman and malvidin-3-galactoside chloride and delphinidin 3-*O*-β-D-glucoside chloride from Sigma-Aldrich) were prepared in DMSO and diluted to 0.5 mg/mL with diethyl pyrocarbonate (DEPC) water. One drop of each solution was set on the top of a sapphire (Al_2O_3) thin slice (with a thickness of 0.5 mm). Absorbance measurements were performed after the solution on the slice was completely dried. The sample-in and sample-out method (Liang, Turnbull, et al. 2022) was used to acquire the spectra, in which the intensity of the light transmitted through the sample ($I(\omega)$) was normalized against the intensity of the light transmitted through an empty area of the sapphire ($I(\omega)$). The absorption spectra were fitted by Gaussian profiles with results given in Supplemental Fig. S21. Data are shown as percentage of its maximum transmission in Fig. 7A.

Phylogenetic analysis

The complete protein sequences of Arabidopsis and grape bHLH subfamily 8 genes were used for phylogenetic reconstruction. Flavonoid-related bHLH subfamily 7 members VviMYC1 and AtTT8 were used as outgroup. Multiple sequence alignments (gap open penalty of −2.9) were performed using the MUSCLE algorithm-based AlignX module from MEGA software (Supplemental File 1). Phylogenetic trees were constructed using the maximum likelihood (ML) method, with partial deletion gap treatments. Reliability of tree nodes was evaluated with 2,000 bootstraps. Resulting tree (Supplemental File 2) was visualized with FigTree (shown in Supplemental Fig. S12).

Statistical analyses

Statistical analyses were carried out using MinitabExpress 1.5.3 software. RT-qPCR data in cv. 'Béquignol' were analyzed

using a 1-way ANOVA to investigate differences between red and white skin areas at each developmental stage. Tukey's post hoc test was used to infer statistically significant means ($P < 0.05$). For gene expression analyses in cv. 'G', 2-way ANOVA was performed to either confirm or rule out interactions between genotypes (treating genotype and light condition together as a single factor) and tissues. Tukey's post hoc test was used to deduce differences between means ($P < 0.1$; $P < 0.05$). Means that do not share a letter are significantly different. Volatilome (targeted) and dual-LUC data were tested for significance using 1-way ANOVA followed by Tukey's post hoc test. Statistical analysis of metabolite, dual-LUC, and gene expression (RT-qPCR) data is provided in Supplemental Data Set 21.

Accession numbers

Sequence data from this article can be found in the Grapedia portal/GeneCards app (https://grapedia.org/genes/) under the following VCost.v3 accession numbers: *MYB24* (Vitvi14g01750), *MYBA1* (Vitvi02g01019), *UFGT1* (Vitvi16g00156), *MYBF1* (Vitvi07g00393), *HYH* (Vitvi05g00274), *FLS1* (Vitvi18g02541), *GT5* (Vitvi11g01290), *TPS35* (Vitvi12g00574), *TPS10* (Vitvi18g02449), *TPS09* (Vitvi18g02448), *HPR1* (Vitvi03g00154), *ACD1* (Vitvi06g00063), *SEN1* (Vitvi04g02160), *PHOT2* (Vitvi03g00272), *sigE* (Vitvi16g01214), *BBX22* (Vitvi12g00543), *FOT6-4* (Vitvi09g00517), *FOT1* (Vitvi02g00475), *SEP2* (Vitvi07g01829), *UVR1* (Vitvi07g01923), *SOD* (Vitvi08g01802), *LPP1* (Vitvi01g01956), *ELIP1* (Vitvi05g00563), *OHP2* (Vitvi18g02961), *PRK* (Vitvi02g00915), *Z-ISO* (Vitvi05g01347), *CRTISO2* (Vitvi12g02046), *LCYE* (Vitvi11g00148), *ZEP1* (Vitvi07g01745), *UBIQUITIN1* (Vitvi16g01364), *EF1* (Vitvi12g02055), and *ACTIN* (Vitvi04g01613). Omics data have been treated and uploaded in public repositories according to the 'Findability, Accessibility, Interoperability, and Reusability' (FAIR) principles, in accordance to the guidelines found at INTEGRAPE website. GCN and DAP-seq data are available at the VitViz platform within the AggGCN and DAPBrowse apps (http://vitviz.tomsbiolab.com/). DAP-seq (GSE198702) and microarray (GSE241123) data are available at NCBI GEO.

Acknowledgments

We thank Joan Marquez-Molins for providing BiFC vectors (NtGFP and CtGFP plasmids) and the technical assistance from Dr. Le Guan, Dr. Lina Wang, and Christel Renaud (INRAE, France) during this work. We also acknowledge Anne-Marie Digby (University of Verona) for language revision. The generation of networks and most bioinformatic analyses were performed on the High Performance Computing (HPC) cluster Garnatxa at the Institute for Integrative Systems Biology (I2SysBio).

Author contributions

J.T.M., Z.D., and F.B. designed the research. C.Z., Z.D., T.F., L.O., A.S.P., A.P., D.C.J.W., C.K., R.L., A.A., B.K., M.L., A.L., Dav.C., C.M.-R., C.E., G.H., R.F.-B., Dar.C., R.A.-G., P.A.-J., P.C., E.D., S.-s.C.H., D.E., and M.R.-C. contributed reagents or conducted experimental/bioinformatic analyses. C.Z., S.S., S.D.C., G.B.T., S.-s.C.H., and J.T.M. analyzed the data. C.Z. and J.T.M. wrote the paper.

Supplemental data

The following materials are available in the online version of this article.

Supplemental Figure S1. The 3 somatic variants of the cv. 'Béquignol' family.

Supplemental Figure S2. Anthocyanin composition in red-skinned variegated and nonvariegated cv. 'B. Noir' berry skins at 5WAV.

Supplemental Figure S3. A selection of significantly enriched terms from KEGG and GO ontologies in RUGs.

Supplemental Figure S4. Expression domains of *MYB24* splicing variants.

Supplemental Figure S5. Several grape sesqui- and monoterpene synthase (*TPS*) genes are highly coexpressed with *MYB24* in late stages of flower and berry development.

Supplemental Figure S6. Expression correlation matrices for MYB24 and isoprenoid/terpenoid genes surveyed in flower and berry developmental samples from high and low terpene-accumulating 'Gewurztraminer' and 'Viognier', respectively.

Supplemental Figure S7. Distribution of MYB24 peaks in the cv. 'Cabernet Sauvignon' CS08 v1.0 genome with respect to all TSS of assigned genes.

Supplemental Figure S8. Preferential binding sites in the *TPS* promoter are specific to MYB24.

Supplemental Figure S9. MYB24 is a nucleus-localized transcriptional activator in vivo.

Supplemental Figure S10. Definition of MYB24 target genes, resulting from the overlap of DAP-seq data (mapped on the PN40024 12X.2 assembly), MYB24 coexpression data (merge of condition-dependent and condition-independent networks), and upregulated genes found in UV-B radiation, drought stress, and/or "light vs shade" transcriptomic studies.

Supplemental Figure S11. Transient expression of *VviMYB24* with *A. thaliana AtMYC5* activates the *VviTPS35* promoter.

Supplemental Figure S12. Phylogenetic analysis and expression of MYC2 and its interaction with MYB24.

Supplemental Figure S13. Regulatory and reciprocal coexpression network of MYB24 and the grape TPS family.

Supplemental Figure S14. Quantification of terpenoid volatiles and the expression patterns of *MYB24* and *TPS35* in the high terpene-accumulating cultivar cv. 'Gewurztraminer' and the low terpene-accumulating cv. 'Viognier'.

Supplemental Figure S15. Correlation analysis between specialized metabolites and mRNA abundances deduced from the integration of transcriptomics/metabolomics data sets from 2 drought-responsive experiments.

Supplemental Figure S16. GC-MS untargeted volatile compound analysis in red and white skin sections of the variegated cv. 'B. Noir' berry.

Supplemental Figure S17. A selection of enriched terms from the MapMan pathway enrichment analysis conducted for (i) all MYB24-bound genes (DAP-seq), (ii) bound genes at −5 kb from TSS, and (iii) HCT (−5 kb to TSS).

Supplemental Figure S18. MYB24 potentially regulates the carotenoid pathway.

Supplemental Figure S19. *MYB24* and *TPS35* expression in response to UV-B irradiation and sunlight/UV-B depletion in greenhouse and field trials.

Supplemental Figure S20. Light-responsiveness of the *MYB24*, *TPS35*, and *HYH* genes in cv. 'G' and 'GF' grape berry tissues.

Supplemental Figure S21. The optical absorbance spectra of flavonols and anthocyanins.

Supplemental Figure S22. Expression profile of some MYB24 targets related to light signaling and photosynthesis.

Supplemental Figure S23. Correlations between different genes in the cv. 'G' experiment.

Supplemental Figure S24. MYBA1 has no effect on the activity of the *TPS35*, *TPS09*, and *HYH* promoters.

Supplemental File 1. MEGA alignment used for bHLH phylogeny.

Supplemental File 2. bHLH phylogenetic newick tree file.

Supplemental Data Set 1. All spotted genes in the Operon array.

Supplemental Data Set 2. Operon oligonucleotide microarrays of variegated red and white skin sections.

Supplemental Data Set 3. DE genes in anthocyanin-depleted sections.

Supplemental Data Set 4. GSEA of RUGs and WUGs.

Supplemental Data Set 5. MapMan enrichment analysis (significantly enriched terms are highlighted in color).

Supplemental Data Set 6. Genes selected to construct the heatmap (Fig. 3C).

Supplemental Data Set 7. MYB24/F1/60 coexpression network analysis in condition-dependent (flower/fruit) and condition-independent (all organs) data (MYB24/F1/60-GCN).

Supplemental Data Set 8. GSEA of MYB24/F1/60-GCN (MYB24/F1/60-GSEA).

Supplemental Data Set 9. The MYB24 DAP-seq results mapped in the CS08 genome.

Supplemental Data Set 10. MYB24-bound TPS genes list from CS08.

Supplemental Data Set 11. Photosynthesis or light-related and isoprenoid/carotenoid-related genes whose promoter regions were bound by MYB24.

Supplemental Data Set 12. MYB24 DAP results mapped in the PN40024 12X.2 assembly, filtered by peak position (−5 kb < distance to TSS < 0).

Supplemental Data Set 13. Coexpression data for MYB24-bound TPS genes that are not in the TOP420 coexpressed list of MYB24-GCN but whose own GCNs include MYB24.

Supplemental Data Set 14. Upregulated genes in 2 berry developmental stages (23° and 26° Brix) in the UV-B studies.

Supplemental Data Set 15. Upregulated genes in 3 berry developmental stages under light vs shade treatments.

Supplemental Data Set 16. Upregulated genes in 2 berry developmental stages (68 and 93 DAA) in the drought studies.

Supplemental Data Set 17. List of putative MYB24 target genes corresponding to the 'Pinot Noir' genome.

Supplemental Data Set 18. MapMan analysis of MYB24-bound genes, bound genes (−5 kb to TSS), and HCT gene list.

Supplemental Data Set 19. Condition-independent metadata list.

Supplemental Data Set 20. Condition-dependent metadata list.

Supplemental Data Set 21. Statistical analysis of the dual-LUC assay.

Supplemental Data Set 22. List of primers used for RT-qPCR analysis.

Funding

This work was supported by grants PGC2018-099449-A-I00 and PID2021-128865NB-I00 and by the Ramón y Cajal program grant RYC-2017-23645, awarded to J.T.M.; PID2021-125575OR-C21 awarded to R.A.-G.; and the FPI scholarship PRE2019-088044 granted to L.O., all from the Ministerio de Ciencia e Innovación (MICINN, Spain), Agencia Estatal de Investigación (AEI, Spain), and Fondo Europeo de Desarrollo Regional (FEDER, European Union). C.Z. is supported by the China Scholarship Council (CSC) no. 201906300087. S.-s.C.H. is partially supported by a National Science Foundation grant PGRP IOS-1916804. This article is based upon work from COST Action CA17111 INTEGRAPE and COST Innovators Grant IG17111 GRAPEDIA, supported by the European Cooperation in Science and Technology (COST).

Conflict of interest statement. None declared.

References

Agati G, Tattini M. Multiple functional roles of flavonoids in photoprotection. New Phytol. 2010:**186**(4):786–793. https://doi.org/10.1111/j.1469-8137.2010.03269.x

Albert NW, Davies KM, Lewis DH, Zhang H, Montefiori M, Brendolise C, Boase MR, Ngo H, Jameson PE, Schwinn KE. A conserved network of transcriptional activators and repressors regulates anthocyanin pigmentation in eudicots. Plant Cell. 2014:**26**(3):962–980. https://doi.org/10.1105/tpc.113.122069

Ampomah-Dwamena C, Thrimawithana AH, Dejnoprat S, Lewis D, Espley RV, Allan AC. A kiwifruit (*Actinidia deliciosa*) R2R3-MYB transcription factor modulates chlorophyll and carotenoid accumulation. New Phytol. 2019:**221**(1):309–325. https://doi.org/10.1111/nph.15362

Apel K, Hirt H. Reactive oxygen species: metabolism, oxidative stress, and signal transduction. Annu Rev Plant Biol.

2004:**55**(1):373–399. https://doi.org/10.1146/annurev.arplant.55.031903.141701

Arnerić M, Traven A, Starešinčić L, Sopta M. The retinoblastoma family of proteins directly represses transcription in *Saccharomyces cerevisiae*. J Biol Chem. 2002:**277**(11):8797–8801. https://doi.org/10.1074/jbc.M111900200

Azuma A, Kobayashi S, Mitani N, Shiraishi M, Yamada M, Ueno T, Kono A, Yakushiji H, Koshita Y. Genomic and genetic analysis of Myb-related genes that regulate anthocyanin biosynthesis in grape berry skin. Theor Appl Genet. 2008:**117**(6):1009–1019. https://doi.org/10.1007/s00122-008-0840-1

Bailey TL, Boden M, Buske FA, Frith M, Grant CE, Clementi L, Ren J, Li WW, Noble WS. MEME Suite: tools for motif discovery and searching. Nucleic Acids Res. 2009:**37**(Web Server):W202–W208. https://doi.org/10.1093/nar/gkp335

Bartlett A, O'Malley RC, Huang SSC, Galli M, Nery JR, Gallavotti A, Ecker JR. Mapping genome-wide transcription-factor binding sites using DAP-seq. Nat Protoc. 2017:**12**(8):1659–1672. https://doi.org/10.1038/nprot.2017.055

Binkert M, Kozma-Bognár L, Terecskei K, De Veylder L, Nagy F, Ulm R. UV-B-responsive association of the Arabidopsis bZIP transcription factor ELONGATED HYPOCOTYL5 with target genes, including its own promoter. Plant Cell. 2014:**26**(10):4200–4213. https://doi.org/10.1105/tpc.114.130716

Bunea CI, Pop N, Babeş AC, Matea C, Dulf FV, Bunea A. Carotenoids, total polyphenols and antioxidant activity of grapes (*Vitis vinifera*) cultivated in organic and conventional systems. Chem Cent J. 2012:**6**(1):66. https://doi.org/10.1186/1752-153X-6-66

Camps C, Kappel C, Lecomte P, Léon C, Gomès E, Coutos-Thévenot P, Delrot S. A transcriptomic study of grapevine (*Vitis vinifera* cv. Cabernet-Sauvignon) interaction with the vascular ascomycete fungus *Eutypa lata*. J Exp Bot. 2010:**61**(6):1719–1737. https://doi.org/10.1093/jxb/erq040

Carbonell-Bejerano P, Diago MP, Martínez-Abaigar J, Martínez-Zapater JM, Tardáguila J, Núñez-Olivera E. Solar ultraviolet radiation is necessary to enhance grapevine fruit ripening transcriptional and phenolic responses. BMC Plant Biol. 2014:**14**(1):1–16. https://doi.org/10.1186/1471-2229-14-183

Carrasco D, De Lorenzis G, Maghradze D, Revilla E, Bellido A, Failla O, Arroyo-García R. Allelic variation in the VvMYBA1 and VvMYBA2 domestication genes in natural grapevine populations (*Vitis vinifera* subsp. *sylvestris*). Plant Syst. Evol. 2015:**301**(6):1613–1624. https://doi.org/10.1007/s00606-014-1181-y

Castellarin SD, Di Gaspero G. Transcriptional control of anthocyanin biosynthetic genes in extreme phenotypes for berry pigmentation of naturally occurring grapevines. BMC Plant Biol. 2007:**7**(1):46. https://doi.org/10.1186/1471-2229-7-46

Cavallini E, Matus JT, Finezzo L, Zenoni S, Loyola R, Guzzo F, Schlechter R, Ageorges A, Arce-Johnson P, Tornielli GB. The phenylpropanoid pathway is controlled at different branches by a set of R2R3-MYB C2 repressors in grapevine. Plant Physiol. 2015:**167**(4):1448–1470. https://doi.org/10.1104/pp.114.256172

Chen Y, Li Y, Narayan R, Subramanian A, Xie X. Gene expression inference with deep learning. Bioinformatics. 2016:**32**(12):1832–1839. https://doi.org/10.1093/bioinformatics/btw074

Cheng H, Song S, Xiao L, Soo HM, Cheng Z, Xie D, Peng J. Gibberellin acts through jasmonate to control the expression of MYB21, MYB24, and MYB57 to promote stamen filament growth in Arabidopsis. PLoS Genet. 2009:**5**(3):e1000440. https://doi.org/10.1371/journal.pgen.1000440

Costantini L, Malacarne G, Lorenzi S, Troggio M, Mattivi F, Moser C, Grando MS. New candidate genes for the fine regulation of the colour of grapes. J Exp Bot. 2015:**66**(15):4427–4440. https://doi.org/10.1093/jxb/erv159

Cravero MC, Guidoni S, Schneider A, Di Stefano R. Morphological and biochemical characterisation of coloured berry-muscat grapevine cultivars. Vitis 1994:**33**(2):75–80.

Czemmel S, Höll J, Loyola R, Arce-Johnson P, Alcalde JA, Matus JT, Bogs J. Transcriptome-wide identification of novel UV-B- and light modulated flavonol pathway genes controlled by VviMYBF1. Front Plant Sci. 2017:**8**:1084. https://doi.org/10.3389/fpls.2017.01084

Czemmel S, Stracke R, Weisshaar B, Cordon N, Harris NN, Walker AR, Robinson SP, Bogs J. The grapevine R2R3-MYB transcription factor VvMYBF1 regulates flavonol synthesis in developing grape berries. Plant Physiol. 2009:**151**(3):1513–1530. https://doi.org/10.1104/pp.109.142059

Dai Z, Meddar M, Renaud C, Merlin I, Hilbert G, Delrot S, Gomès E. Long-term in vitro culture of grape berries and its application to assess the effects of sugar supply on anthocyanin accumulation. J Exp Bot. 2014:**65**(16):4665–4677. https://doi.org/10.1093/jxb/ert489

Downey MO, Harvey JS, Robinson SP. Synthesis of flavonols and expression of flavonol synthase genes in the developing grape berries of Shiraz and Chardonnay (*Vitis vinifera* L). Aust. J. Grape Wine Res. 2003:**9**(2):110–121. https://doi.org/10.1111/j.1755-0238.2003.tb00261.x

Espley RV, Brendolise C, Chagné D, Kutty-Amma S, Green S, Volz R, Putterill J, Schouten HJ, Gardiner SE, Hellens RP, et al. Multiple repeats of a promoter segment causes transcription factor autoregulation in red apples. Plant Cell. 2009:**21**(1):168–183. https://doi.org/10.1105/tpc.108.059329

Fasoli M, Dal Santo S, Zenoni S, Tornielli GB, Farina L, Zamboni A, Porceddu A, Venturini L, Bicego M, Murino V, et al. The grapevine expression atlas reveals a deep transcriptome shift driving the entire plant into a maturation program. Plant Cell. 2012:**24**(9):3489–3505. https://doi.org/10.1105/tpc.112.100230

Ferreira V, Castro I, Carrasco D, Pinto-Carnide O, Arroyo-García R. Molecular characterization of berry skin color reversion on grape somatic variants. J Berry Res. 2018:**8**(3):147–162. https://doi.org/10.3233/JBR-170289

Ferreira V, Pinto-Carnide O, Arroyo-García R, Castro I. Berry color variation in grapevine as a source of diversity. Plant Physiol Biochem. 2018:**132**:696–707. https://doi.org/10.1016/j.plaphy.2018.08.021

Foster TM, Aranzana MJ. Attention sports fans! the far-reaching contributions of bud sport mutants to horticulture and plant biology. Hortic Res. 2018:**5**(1):44. https://doi.org/10.1038/s41438-018-0062-x

Fournier-Level A, Le Cunff L, Gomez C, Doligez A, Ageorges A, Roux C, Bertrand Y, Souquet JM, Cheynier V, This P. Quantitative genetic bases of anthocyanin variation in grape (*Vitis vinifera* L. ssp. *sativa*) berry: a quantitative trait locus to quantitative trait nucleotide integrated study. Genetics 2009:**183**(3):1127–1139. https://doi.org/10.1534/genetics.109.103929

Frank MH, Chitwood DH. Plant chimeras: the good, the bad, and the 'Bizzaria'. Dev Biol. 2016:**419**(1):41–53. https://doi.org/10.1016/j.ydbio.2016.07.003

Friedel M, Frotscher J, Nitsch M, Hofmann M, Bogs J, Stoll M, Dietrich H. Light promotes expression of monoterpene and flavonol metabolic genes and enhances flavour of winegrape berries (*Vitis vinifera* L. cv. Riesling). Aust J Grape Wine Res. 2016:**22**(3):409–421. https://doi.org/10.1111/ajgw.12229

Galbiati M, Matus JT, Francia P, Rusconi F, Cañón P, Medina C, Conti L, Cominelli E, Tonelli C, Arce-Johnson P. The grapevine guard cell-related VvMYB60 transcription factor is involved in the regulation of stomatal activity and is differentially expressed in response to ABA and osmotic stress. BMC Plant Biol. 2011:**11**(1):1–15. https://doi.org/10.1186/1471-2229-11-142

Gentleman RC, Carey VJ, Bates DM, Bolstad B, Dettling M, Dudoit S, Ellis B, Gautier L, Ge Y, Gentry J, et al. Bioconductor: open software development for computational biology and bioinformatics. Genome Biol. 2004:**5**(10):R80. https://doi.org/10.1186/gb-2004-5-10-r80

Goss R, Lepetit B. Biodiversity of NPQ. J. Plant Physiol. 2015:**172**:13–32. https://doi.org/10.1016/j.jplph.2014.03.004

Guan L, Dai Z, Wu BH, Wu J, Merlin I, Hilbert G, Renaud C, Gomès E, Edwards E, Li SH, et al. Anthocyanin biosynthesis is differentially

regulated by light in the skin and flesh of white-fleshed and teinturier grape berries. Planta 2016:**243**(1):23–41. https://doi.org/10.1007/s00425-015-2391-4

Guo Y, Mahony S, Gifford DK. High resolution genome wide binding event finding and motif discovery reveals transcription factor spatial binding constraints. PLoS Comput Biol. 2012:**8**(8):e1002638. https://doi.org/10.1371/journal.pcbi.1002638

Harari-Steinberg O, Ohad I, Chamovitz DA. Dissection of the light signal transduction pathways regulating the two early light-induced protein genes in Arabidopsis. Plant Physiol. 2001:**127**(3):986–997. https://doi.org/10.1104/pp.010270

Hichri I, Heppel SC, Pillet J, Léon C, Czemmel S, Delrot S, Lauvergeat V, Bogs J. The basic helix-loop-helix transcription factor MYC1 is involved in the regulation of the flavonoid biosynthesis pathway in grapevine. Mol Plant. 2010:**3**(3):509–523. https://doi.org/10.1093/mp/ssp118

Hilbert G, Temsamani H, Bordenave L, Pedrot E, Chaher N, Cluzet S, Delaunay JC, Ollat N, Delrot S, Mérillon JM, et al. Flavonol profiles in berries of wild Vitis accessions using liquid chromatography coupled to mass spectrometry and nuclear magnetic resonance spectrometry. Food Chem. 2015:**169**:49–58. https://doi.org/10.1016/j.foodchem.2014.07.079

Huang J, Zhao X, Chory J. The Arabidopsis transcriptome responds specifically and dynamically to high light stress. Cell Rep. 2019:**29**(12):4186–4199.e3. https://doi.org/10.1016/j.celrep.2019.11.051

Jaillon O, Aury JM, Noel B, Policriti A, Clepet C, Casagrande A, Choisne N, Aubourg S, Vitulo N, Jubin C, et al. The grapevine genome sequence suggests ancestral hexaploidization in major angiosperm phyla. Nature 2007:**449**(7161):463–467. https://doi.org/10.1038/nature06148

Joubert C, Young PR, Eyéghé-Bickong HA, Vivier MA. Field-grown grapevine berries use carotenoids and the associated xanthophyll cycles to acclimate to UV exposure differentially in high and low light (shade) conditions. Front Plant Sci. 2016:**7**:786. https://doi.org/10.3389/fpls.2016.00786

Kelemen Z, Sebastian A, Xu W, Grain D, Salsac F, Avon A, Berger N, Tran J, Dubreucq B, Lurin C, et al. Analysis of the DNA-binding activities of the Arabidopsis R2R3-MYB transcription factor family by one-hybrid experiments in yeast. PLoS One 2015:**10**(10):e0141044. https://doi.org/10.1371/journal.pone.0141044

Kersey PJ, Allen JE, Christensen M, Davis P, Falin LJ, Grabmueller C, Hughes DST, Humphrey J, Kerhornou A, Khobova J, et al. Ensembl Genomes 2013: scaling up access to genome-wide data. Nucleic Acids Res. 2014:**42**(D1):D546–D552. https://doi.org/10.1093/nar/gkt979

Kim J, DellaPenna D. Defining the primary route for lutein synthesis in plants: the role of Arabidopsis carotenoid β-ring hydroxylase CYP97A3. Proc Natl Acad Sci U S A. 2006:**103**(9):3474–3479. https://doi.org/10.1073/pnas.0511207103

Knapp A, Carter G. Variability in leaf optical properties among 26 species from a broad range of habitats. Am J Bot. 1998:**85**(7):940–946. https://doi.org/10.2307/2446360

Kobayashi S, Goto-Yamamoto N, Hirochika H. Retrotransposon-induced mutations in grape skin color. Science 2004:**304**(5673):982. https://doi.org/10.1126/science.1095011

Kovalenko Y, Tindjau R, Madilao LL, Castellarin SD. Regulated deficit irrigation strategies affect the terpene accumulation in Gewürztraminer (*Vitis vinifera* L.) grapes grown in the Okanagan Valley. Food Chem. 2021:**341**:128172. https://doi.org/10.1016/j.foodchem.2020.128172

Langfelder P, Horvath S. WGCNA: an R package for weighted correlation network analysis. BMC Bioinformatics. 2008:**9**(1):559. https://doi.org/10.1186/1471-2105-9-559

Lee GW, Lee S, Chung MS, Jeong YS, Chung BY. Rice terpene synthase 20 (OsTPS20) plays an important role in producing terpene volatiles in response to abiotic stresses. Protoplasma 2015:**252**(4):997–1007. https://doi.org/10.1007/s00709-014-0735-8

Lee J, He K, Stolc V, Lee H, Figueroa P, Gao Y, Tongprasit W, Zhao H, Lee I, Deng XW. Analysis of transcription factor HY5 genomic binding sites revealed its hierarchical role in light regulation of development. Plant Cell. 2007:**19**(3):731–749. https://doi.org/10.1105/tpc.106.047688

Liang A, Rodríguez F, Rodríguez-Hernandez P, Muñoz A, Turnbull R, Errandonea D. High-pressure tuning of *d-d* crystal-field electronic transitions and electronic band gap in $Co(IO_3)_2$. Phys Rev B. 2022:**105**(11):115204. https://doi.org/10.1103/PhysRevB.105.115204

Liang A, Turnbull R, Rodríguez-Hernandez P, Muñoz A, Jasmin M, Shi LT, Errandonea D. General relationship between the band-gap energy and iodine-oxygen bond distance in metal iodates. Phys Rev Mater. 2022:**6**(4):044603. https://doi.org/10.1103/PhysRevMaterials.6.044603

Lijavetzky D, Ruiz-García L, Cabezas JA, De Andrés MT, Bravo G, Ibáñez A, Carreño J, Cabello F, Ibáñez J, Martínez-Zapater JM. Molecular genetics of berry colour variation in table grape. Mol Genet Genomics. 2006:**276**(5):427–435. https://doi.org/10.1007/s00438-006-0149-1

Liu G, Ren G, Guirgis A, Thornburg RW. The MYB305 transcription factor regulates expression of nectarin genes in the ornamental tobacco floral nectary. Plant Cell. 2009:**21**(9):2672–2687. https://doi.org/10.1105/tpc.108.060079

Lloyd A, Brockman A, Aguirre L, Campbell A, Bean A, Cantero A, Gonzalez A. Advances in the MYB-bHLH-WD repeat (MBW) pigment regulatory model: addition of a WRKY factor and co-option of an anthocyanin MYB for betalain regulation. Plant Cell Physiol. 2017:**58**(9):1431–1441. https://doi.org/10.1093/pcp/pcx075

Lodhi MA, Ye GN, Weeden NF, Reisch BI. A simple and efficient method for DNA extraction from grapevine cultivars and Vitis species. Plant Mol Biol Rep. 1994:**12**(1):6–13. https://doi.org/10.1007/BF02668658

Long M, Millar DJ, Kimura Y, Donovan G, Rees J, Fraser PD, Bramley PM, Bolwell GP. Metabolite profiling of carotenoid and phenolic pathways in mutant and transgenic lines of tomato: identification of a high antioxidant fruit line. Phytochemistry 2006:**67**(16):1750–1757. https://doi.org/10.1016/j.phytochem.2006.02.022

Loyola R, Herrera D, Mas A, Wong DCJ, Höll J, Cavallini E, Amato A, Azuma A, Ziegler T, Aquea F, et al. The photomorphogenic factors UV-B RECEPTOR 1, ELONGATED HYPOCOTYL 5, and HY5 HOMOLOGUE are part of the UV-B signalling pathway in grapevine and mediate flavonol accumulation in response to the environment. J Exp Bot. 2016:**67**(18):5429–5445. https://doi.org/10.1093/jxb/erw307

Lu S, Wang J, Zhuge Y, Zhang M, Liu C, Jia H, Fang J. Integrative analyses of metabolomes and transcriptomes provide insights into flavonoid variation in grape berries. J Agric Food Chem. 2021:**69**(41):12354–12367. https://doi.org/10.1021/acs.jafc.1c02703

Marcotrigiano M. Chimeras and variegation: patterns of deceit. HortScience 1997:**32**(5):773–784. https://doi.org/10.21273/HORTSCI.32.5.773

Martin DM, Aubourg S, Schouwey MB, Daviet L, Schalk M, Toub O, Lund ST, Bohlmann J. Functional annotation, genome organization and phylogeny of the grapevine (*Vitis vinifera*) terpene synthase gene family based on genome assembly, FLcDNA cloning, and enzyme assays. BMC Plant Biol. 2010:**10**(1):226. https://doi.org/10.1186/1471-2229-10-226

Martin DM, Fäldt J, Bohlmann J. Functional characterization of nine Norway spruce TPS genes and evolution of gymnosperm terpene synthases of the TPS-d subfamily. Plant Physiol. 2004:**135**:1908–1927.

Martínez-Lüscher J, Sánchez-Díaz M, Delrot S, Aguirreolea J, Pascual I, Gomès E. Ultraviolet-B radiation and water deficit interact to alter flavonol and anthocyanin profiles in grapevine berries through transcriptomic regulation. Plant Cell Physiol. 2014:**55**(11):1925–1936. https://doi.org/10.1093/pcp/pcu121

Massonnet M, Fasoli M, Tornielli GB, Altieri M, Sandri M, Zuccolotto P, Paci P, Gardiman M, Zenoni S, Pezzotti M. Ripening transcriptomic program in red and white grapevine varieties correlates with berry skin anthocyanin accumulation. Plant Physiol. 2017:**174**(4):2376–2396. https://doi.org/10.1104/pp.17.00311

Matus JT, Cavallini E, Loyola R, Höll J, Finezzo L, Dal Santo S, Vialet S, Commisso M, Roman F, Schubert A, et al. A group of grapevine MYBA transcription factors located in chromosome 14 control anthocyanin synthesis in vegetative organs with different specificities compared with the berry color locus. Plant J. 2017:**91**(2):220–236. https://doi.org/10.1111/tpj.13558

Matus JT, Loyola R, Vega A, Peña-Neira A, Bordeu E, Arce-Johnson P, Alcalde JA. Post-veraison sunlight exposure induces MYB-mediated transcriptional regulation of anthocyanin and flavonol synthesis in berry skins of *Vitis vinifera*. J Exp Bot. 2009:**60**(3):853–867. https://doi.org/10.1093/jxb/ern336

Merdinoglu D, Butterlin G, Bevilacqua L, Chiquet V, Adam-Blondon AF, Decroocq S. Development and characterization of a large set of microsatellite markers in grapevine (*Vitis vinifera* L.) suitable for multiplex PCR. Mol Breed. 2005:**15**(4):349–366. https://doi.org/10.1007/s11032-004-7651-0

Mori K, Goto-Yamamoto N, Kitayama M, Hashizume K. Loss of anthocyanins in red-wine grape under high temperature. J Exp Bot. 2007:**58**(8):1935–1945. https://doi.org/10.1093/jxb/erm055

Mutwil M, Klie S, Tohge T, Giorgi FM, Wilkins O, Campbell MM, Fernie AR, Usadel B, Nikoloski Z, Persson S. Planet: combined sequence and expression comparisons across plant networks derived from seven species. Plant Cell. 2011:**23**(3):895–910. https://doi.org/10.1105/tpc.111.083667

Navarro JA, Serra-Soriano M, Corachán-Valencia L, Pallás V. A conserved motif in three viral movement proteins from different genera is required for host factor recruitment and cell-to-cell movement. Sci Rep. 2020:**10**(1):4758. https://doi.org/10.1038/s41598-020-61741-5

Navarro-Payá D, Santiago A, Orduña L, Zhang C, Amato A, D'Inca E, Fattorini C, Pezzotti M, Tornielli GB, Zenoni S, et al. The grape gene reference catalogue as a standard resource for gene selection and genetic improvement. Front Plant Sci. 2022:**12**:3324. https://doi.org/10.3389/fpls.2021.803977

Novikov E, Barillot E. Software package for automatic microarray image analysis (MAIA). Bioinformatics. 2007:**23**(5):639–640. https://doi.org/10.1093/bioinformatics/btl644

O'Malley RC, Huang SSC, Song L, Lewsey MG, Bartlett A, Nery JR, Galli M, Gallavotti A, Ecker JR. Cistrome and epicistrome features shape the regulatory DNA landscape. Cell 2016:**165**(5):1280–1292. https://doi.org/10.1016/j.cell.2016.04.038

Orduña L, Li M, Navarro-Payá D, Zhang C, Santiago A, Romero P, Ramšak Ž, Magon G, Höll J, Merz P, et al. Direct regulation of shikimate, early phenylpropanoid, and stilbenoid pathways by subgroup 2 R2R3-MYBs in grapevine. Plant J. 2022:**10**(2):529–547. https://doi.org/10.1111/tpj.15686

Orduña L, Santiago A, Navarro-Paya D, Zhang C, Wong DC, Matus JT. Aggregated gene co-expression networks for predicting transcription factor regulatory landscapes in a non-model plant species. bioRxiv. 2023.

Pastore C, Zenoni S, Fasoli M, Pezzotti M, Tornielli GB, Filippetti I. Selective defoliation affects plant growth, fruit transcriptional ripening program and flavonoid metabolism in grapevine. BMC Plant Biol. 2013:**13**(1):30. https://doi.org/10.1186/1471-2229-13-30

Pellerone FI, Edwards KJ, Thomas MR. Grapevine microsatellite repeats: isolation, characterisation and use for genotyping of grape germplasm from southern Italy. Vitis 2001:**40**(4):179–186.

Qi T, Huang H, Song S, Xie D. Regulation of jasmonate-mediated stamen development and seed production by a bHLH-MYB complex in Arabidopsis. Plant Cell. 2015:**27**(6):1620–1633. https://doi.org/10.1105/tpc.15.00116

Reeves PH, Ellis CM, Ploense SE, Wu M-F, Yadav V, Tholl D, Chételat A, Haupt I, Kennerley BJ, Hodgens C, et al. A regulatory network for coordinated flower maturation. PLoS Genet. 2012:**8**(2):e1002506. https://doi.org/10.1371/journal.pgen.1002506

Reid KE, Olsson N, Schlosser J, Peng F, Lund ST. An optimized grapevine RNA isolation procedure and statistical determination of reference genes for real-time RT-PCR during berry development. BMC Plant Biol. 2006:**6**(1):27. https://doi.org/10.1186/1471-2229-6-27

Richaud D, Stange C, Gadaleta A, Colasuonno P, Parada R, Schwember AR. Identification of lycopene epsion cyclase (LCYE) gene mutants to potentially increase β-carotene content in durum wheat (*Triticum turgidum* L. ssp *Durum*) through TILLING. PLoS One 2018:**13**(12):e0208948. https://doi.org/10.1371/journal.pone.0208948

Ritchie ME, Silver J, Oshlack A, Holmes M, Diyagama D, Holloway A, Smyth GK. A comparison of background correction methods for two-colour microarrays. Bioinformatics. 2007:**23**(20):2700–2707. https://doi.org/10.1093/bioinformatics/btm412

Rodríguez-Lorenzo M, Mauri N, Royo C, Rambla JL, Diretto G, Demurtas O, Hilbert G, Renaud C, Tobar V, Huete J, et al. The flavour of grape colour: anthocyanin content tunes aroma precursor composition by altering the berry microenvironment. J Exp Bot. 2023:erad223. https://doi.org/10.1093/jxb/erad223

Rotter A, Camps C, Lohse M, Kappel C, Pilati S, Hren M, Stitt M, Coutos-Thévenot P, Moser C, Usadel B, et al. Gene expression profiling in susceptible interaction of grapevine with its fungal pathogen *Eutypa lata*: extending MapMan ontology for grapevine. BMC Plant Biol. 2009:**9**(1):104. https://doi.org/10.1186/1471-2229-9-104

Ruban AV. Nonphotochemical chlorophyll fluorescence quenching: mechanism and effectiveness in protecting plants from photodamage. Plant Physiol. 2016:**170**(4):1903–1916. https://doi.org/10.1104/pp.15.01935

Sagawa JM, Stanley LE, Lafountain AM, Frank HA, Liu C, Yuan YW. An R2R3-MYB transcription factor regulates carotenoid pigmentation in *Mimulus lewisii* flowers. New Phytol. 2016:**209**(3):1049–1057. https://doi.org/10.1111/nph.13647

Santibáñez C, Meyer C, Martínez L, Moyano T, Lunn J, Feil R, Dai Z, Carrasco D, Arroyo-García R, Hilbert G, et al. Differences in berry primary and secondary metabolisms identified by transcriptomic and metabolic profiling of two table grape color somatic variants. bioRxiv. 2019.

Savoi S, Wong DCJ, Arapitsas P, Miculan M, Bucchetti B, Peterlunger E, Fait A, Mattivi F, Castellarin SD. Transcriptome and metabolite profiling reveals that prolonged drought modulates the phenylpropanoid and terpenoid pathway in white grapes (*Vitis vinifera* L.). BMC Plant Biol. 2016:**16**(1):67. https://doi.org/10.1186/s12870-016-0760-1

Savoi S, Wong DCJ, Degu A, Herrera JC, Bucchetti B, Peterlunger E, Fait A, Mattivi F, Castellarin SD. Multi-omics and integrated network analyses reveal new insights into the systems relationships between metabolites, structural genes, and transcriptional regulators in developing grape berries (*Vitis vinifera* L.) exposed to water deficit. Front Plant Sci. 2017:**8**:1124. https://doi.org/10.3389/fpls.2017.01124

Schöttler MA, Tóth SZ. Photosynthetic complex stoichiometry dynamics in higher plants: environmental acclimation and photosynthetic flux control. Front Plant Sci. 2014:**5**:188. https://doi.org/10.3389/fpls.2014.00188

Sharma PK, Hall DO. Effect of high-irradiance stress on primary photochemistry and light regulated enzymes of photosynthetic carbon metabolism. J Plant Physiol. 1992:**139**(6):719–726. https://doi.org/10.1016/S0176-1617(11)81717-7

Smit SJ, Vivier MA, Young PR. Seeing the forest through the (phylogenetic) trees: functional characterisation of grapevine terpene synthase (VviTPS) paralogues and orthologues. Plants 2021:**10**(8):1520. https://doi.org/10.3390/plants10081520

Smyth GK. Linear models and empirical Bayes methods for assessing differential expression in microarray experiments. Stat Appl Genet Mol Biol. 2004:**3**(1):1–25. https://doi.org/10.2202/1544-6115.1027

Smyth GK, Speed T. Normalization of cDNA microarray data. Methods 2003:**31**(4):265–273. https://doi.org/10.1016/S1046-2023(03)00155-5

Stapleton AE, Walbot V. Flavonoids can protect maize DNA from the induction of ultraviolet radiation damage. Plant Physiol. 1994:**105**(3):881–889. https://doi.org/10.1104/pp.105.3.881

Subramanian A, Tamayo P, Mootha VK, Mukherjee S, Ebert BL, Gillette MA, Paulovich A, Pomeroy SL, Golub TR, Lander ES, et al. Gene set enrichment analysis: a knowledge-based approach for interpreting genome-wide expression profiles. Proc Natl Acad Sci U S A. 2005:**102**(43):15545–15550. https://doi.org/10.1073/pnas.0506580102

Sun RZ, Cheng G, Li Q, He Y-N, Wang Y, Lan Y-B, Li S-Y, Zhu Y-R, Song W-F, Zhang X, et al. Light-induced variation in phenolic compounds in cabernet sauvignon grapes (*Vitis vinifera* L.) involves extensive transcriptome reprogramming of biosynthetic enzymes, transcription factors, and phytohormonal regulators. Front. Plant Sci. 2017:**8**:547. https://doi.org/10.3389/fpls.2017.00547

Suzek BE, Huang H, McGarvey P, Mazumder R, Wu CH. Uniref: comprehensive and non-redundant UniProt reference clusters. Bioinformatics. 2007:**23**(10):1282–1288. https://doi.org/10.1093/bioinformatics/btm098

Thimm O, Bläsing O, Gibon Y, Nagel A, Meyer S, Krüger P, Selbig J, Müller LA, Rhee SY, Stitt M. MAPMAN: a user-driven tool to display genomics data sets onto diagrams of metabolic pathways and other biological processes. Plant J. 2004:**37**(6):914–939. https://doi.org/10.1111/j.1365-313X.2004.02016.x

Thomas MR, Matsumoto S, Cain P, Scott NS. Repetitive DNA of grapevine: classes present and sequences suitable for cultivar identification. Theor Appl Genet. 1993:**86**(2–3):173–180. https://doi.org/10.1007/BF00222076

Toledo-Ortiz G, Huq E, Quail PH. The Arabidopsis basic/helix-loop-helix transcription factor family. Plant Cell. 2003:**15**(8):1749–1770. https://doi.org/10.1105/tpc.013839

Vannozzi A, Wong DCJ, Höll J, Hmmam I, Matus JT, Bogs J, Ziegler T, Dry I, Barcaccia G, Lucchin M. Combinatorial regulation of stilbene synthase genes by WRKY and MYB transcription factors in grapevine (*Vitis vinifera* L.). Plant Cell Physiol. 2018:**59**(5):1043–1059. https://doi.org/10.1093/pcp/pcy045

Verweij W, Spelt CE, Bliek M, de Vries M, Wit N, Faraco M, Koes R, Quattrocchio FM. Functionally similar WRKY proteins regulate vacuolar acidification in petunia and hair development in Arabidopsis. Plant Cell. 2016:**28**(3):786–803. https://doi.org/10.1105/tpc.15.00608

Vezzulli S, Leonardelli L, Malossini U, Stefanini M, Velasco R, Moser C. Pinot blanc and Pinot gris arose as independent somatic mutations of Pinot noir. J Exp Bot. 2012:**63**:6359–6369.

Wade Harper J, Adami GR, Wei N, Keyomarsi K, and Elledge SJ. The p21 Cdk-interacting protein Cip1 is a potent inhibitor of G1 cyclin-dependent kinases. Cell 1993:**75**(4):805–816. https://doi.org/10.1016/0092-8674(93)90499-G

Walker AR, Lee E, Bogs J, McDavid DAJ, Thomas MR, Robinson SP. White grapes arose through the mutation of two similar and adjacent regulatory genes. Plant J. 2007:**49**(5):772–785. https://doi.org/10.1111/j.1365-313X.2006.02997.x

Walker AR, Lee E, Robinson SP. Two new grape cultivars, bud sports of Cabernet Sauvignon bearing pale-coloured berries, are the result of deletion of two regulatory genes of the berry colour locus. Plant Mol Biol. 2006:**62**:623–635.

Walters RG. Towards an understanding of photosynthetic acclimation. J Exp Bot. 2005:**56**(411):435–447. https://doi.org/10.1093/jxb/eri060

Wen YQ, Zhong GY, Gao Y, Lan YB, Duan CQ, Pan QH. Using the combined analysis of transcripts and metabolites to propose key genes for differential terpene accumulation across two regions. BMC Plant Biol. 2015:**15**(1):240. https://doi.org/10.1186/s12870-015-0631-1

Winkel-Shirley B. Biosynthesis of flavonoids and effects of stress. Curr Opin Plant Biol. 2002:**5**(3):218–223. https://doi.org/10.1016/S1369-5266(02)00256-X

Wong DCJ, Schlechter R, Vannozzi A, Höll J, Hmmam I, Bogs J, Tornielli GB, Castellarin SD, Matus JT. A systems-oriented analysis of the grapevine R2R3-MYB transcription factor family uncovers new insights into the regulation of stilbene accumulation. DNA Res. 2016:**23**(5):451–466. https://doi.org/10.1093/dnares/dsw028

Wu M, Xu X, Hu X, Liu Y, Cao H, Chan H, Gong Z, Yuan Y, Luo Y, Feng B, et al. SlMYB72 regulates the metabolism of chlorophylls, carotenoids, and flavonoids in tomato fruit. Plant Physiol. 2020:**183**(3):854–868. https://doi.org/10.1104/pp.20.00156

Yang Z, Li Y, Gao F, Jin W, Li S, Kimani S, Yang S, Bao T, Gao X, Wang L. MYB21 interacts with MYC2 to control the expression of terpene synthase genes in flowers of *Freesia hybrida* and *Arabidopsis thaliana*. J Exp Bot. 2020:**71**(14):4140–4158. https://doi.org/10.1093/jxb/eraa184

Young PR, Lashbrooke JG, Alexandersson E, Jacobson D, Moser C, Velasco R, Vivier MA. The genes and enzymes of the carotenoid metabolic pathway in *Vitis vinifera* L. BMC Genomics. 2012:**13**(1):243. https://doi.org/10.1186/1471-2164-13-243

Zhang E, Chai F, Zhang H, Li S, Liang Z, Fan P. Effects of sunlight exclusion on the profiles of monoterpene biosynthesis and accumulation in grape exocarp and mesocarp. Food Chem. 2017:**237**:379–389. https://doi.org/10.1016/j.foodchem.2017.05.127

Zheng T, Guan L, Yu K, Haider MS, Nasim M, Liu Z, Li T, Zhang K, Jiu S, Jia H, et al. Expressional diversity of grapevine 3-hydroxy-3-methylglutaryl-CoA reductase (VvHMGR) in different grapes genotypes. BMC Plant Biol. 2021:**21**(1):279. https://doi.org/10.1186/s12870-021-03073-8

Zuo Z, Wang B, Ying B, Zhou L, Zhang R. Monoterpene emissions contribute to thermotolerance in *Cinnamomum camphora*. Trees Struct Funct. 2017:**31**(6):1759–1771. https://doi.org/10.1007/s00468-017-1582-y